TIME-WINDOWED BLOCK FOR UNMYELINATED FIBERS IN THE SCIATIC NERVE OF THE FROG

by

Samet KOCATÜRK

BS, Electrical Engineering, Yıldız Technical University, 2010

Submitted to the Institute of Biomedical Engineering
in partial fulfillment of the requirements
for the degree of
Master of Science
in
Biomedical Engineering

Boğaziçi University
2015

Academic Ethics and Integrity Statement

(To be completed upon submission of Master and PhD Theses for examination)

I am familiar with the YÖK (Higher Council of Education) Academic Ethics and Integrity Policy and I understand the potential consequences should my thesis be found to contain plagiarized content or violate this policy in any other way.

Name: ..... Date: .....

Signature: .....

ACKNOWLEDGMENTS

I'm grateful to my family for their support and encouragement during my master study.

I specially thank to my advisor Burak Güçlü for his support, help and motivation during all stages of the thesis.

I thank to Prof. Dr. Mehmed Özkan and Assist. Prof. Pınar Öz for their precious comments.

I also thank to my labmates İsmail Devecioğlu, Bige Vardar, Sedef Yusufoğulları, Sevgi Öztürk, Deniz Kılınç, İpel Toker, Emre Canayaz and my friends.

ABSTRACT

TIME-WINDOWED BLOCK FOR UNMYELINATED FIBERS IN THE SCIATIC NERVE OF THE FROG

An artificial sensation can be produced in neuroprotheses by functional electrical stimulation of the sensory fibers in the peripheral nerves. The stimulation amplitude has effects on the perceptive field and the sensation modality. Increase beyond a certain threshold causes annoying sensations such as itch and pain. In this thesis, a novel method is proposed to improve this problem by blocking these unwanted sensations.

In this study, a DC hyperpolarizing stimulation with a subsequent exponential decay was employed to block the conduction of C fibers of the frog's sciatic nerve. The block was applied in a time window to allow the propagation in myelinated fibers. The neural activity was measured by CAPs. For the blocking stimulus, two delays (4, 6 ms), three durations (4, 6, 8 ms), and five amplitude levels relative to the excitation threshold of C fibers were used. The excitation characteristics were also measured.

In the CAP traces, the C component was reduced in 44% of the valid trials (n=67). The valid trials were the recordings in which the blocking stimulation did not evoke activity in myelinated fibers. After aligned-rank transform, 2-way ANOVA was performed to test the effects of block duration and amplitude on the reduction of C components. There were no significant effect of block duration (p=0.87) and amplitude (p=0.12). There was also no significant interaction between block duration and amplitude. Data from all trials (n=292) were included in Pearson correlation analysis to test the change of activity in the CAP component from myelinated fibers due to electrical charge applied by the blocking stimulation and there was no correlation (p=0.7).

According to these results, the performance of neuroprostheses can be improved by a hyperpolarization block. Although the C fibers could not be blocked in all trials, when they did, the activity in the myelinated fibers was not significantly affected.

Keywords: C Fiber, Unmyelinated, Frog, Hyperpolarization, Anodal, DC, Block.

ÖZET

KURBAĞDA SİYATİK SİNİRİNDEKİ MİYELİNSİZ LİFLERİN ZAMANDA PENCERE YÖNTEMİ İLE BLOKLANMASI

Çevresel sinirlerdeki duyu liflerinin elektriksel uyarılması ile nöroprotezlerde suni duyu bilgisinin oluşturulabileceği gösterilmiştir. Uyarı genliği arttıkça, oluşan suni duyar alan ve duyu modalitesi de değişebilmektedir. Belli bir eşiğin üzerine çıkıldığında ise kaşıntı ve acı gibi rahatsız hisler oluşabilmektedir. Bu çalışmada bu istenmeyen hislerin giderilmesi için yeni bir yöntem önerilmektedir.

Deneylerde kurbağanın siyatik sinirinin uyarılması ile etkinleşen C liflerinin iletimi DC hiperpolarize blok uyarı kullanılarak azaltılmıştır. Blok uyaranı miyelinli liflerin iletimini bozmayacak şekilde belirli bir zaman penceresinde uygulanmıştır. Sinir aktivitesi bileşik aksiyon potansiyelleri kayıt edilerek ölçülmüştür. Blok uyaran iki gecikme süresi (4, 6 ms), üç uyarı süresi (4, 6, 8 ms) ve beş genlik seviyesinde verilmiştir. Ayrıca miyelinli ve C liflerinin fizyolojik uyarılma özellikleri belirlenmiştir.

Bileşik aksiyon potansiyeli kayıtlarında C bileşeninin geçerli denemelerin (n=67) sadece %44' ünde azaldığı bulunmuştur. Geçerli denemeler olarak blok uyaranın miyelinli lifleri uyarmadığı denemeler analiz edilmiştir. Düzeltilmiş rank dönüşümü uygulandıktan sonra 2 yollu ANOVA kullanılarak blok süresinin ve genliğinin C bileşenini azaltması incelenmiştir. İstatiksel olarak blok süresinin (p=0.87) ve genliğinin (p=0.12) anlamlı bir etkisinin olmadığı bulunmuştur. Aynı zamanda bu iki faktör arasında da bir etkileşim bulunamamıştır. Bütün denemelerden elde edilen veriler birleştirilerek (n=292) blok uyaran nedeniyle oluşan elektriksel yük ile miyelinli liflerin aktivitesindeki değişim arasında Pearson korelasyon analizi ile anlamlı bir korelasyon bulunmamıştır.

Tezde elde edilen sonuçlar nöroprotezlerin duyusal özelliklerinin hiperpolarizasyon blok yardımıyla iyileştirilebileceğini göstermektedir. C lifleri bütün denemelerde bloklanmadığı halde, bloklanan denemelerde miyelinli liflerin pek etkilenmediği görülmektedir. Yöntemdeki kısıtlamalar detaylı olarak incelenmiştir.

Anahtar Sözcükler: C Fiber, Miyelinsiz, Kurbağa, Hiperpolarizasyon, Anodal, Blok.

TABLE OF CONTENTS

LIST OF FIGURES

LIST OF TABLES

LIST OF SYMBOLS

I	Current
I_{rh}	Rheobase
A	Amper
Q	Charge
C	Coulomb
t	Time
μ	Micro
τ_{SD}	Chronaxie

LIST OF ABBREVIATIONS

CAP	Compound Action Potential
FES	Functional Electrical Stimulation
RMS	Root Mean Square
S-D	Strength Duration
DC	Direct Current
AC	Alternating Current
Std	Standard Deviation
LPF	Low Pass Filter
HPF	High Pass Filter
CNS	Central Nervous System
PNS	Peripheral Nervous System

1. INTRODUCTION

1.1 Motivation

The nervous system is the main information processing system of the body. It collects information about the body and the environment and reacts according to these inputs. The functioning of the nervous system can be distorted by a disease or a physical damage. Recovery of the nervous system is generally very little or none. When the peripheral nervous system is considered, one of the worst case scenarios is the loss of extremities at different levels. The estimated number of amputees in US is approximately 1.2 million in 1996 and thousands of people undergo upper limb or lower limb amputation [1].

Different procedures exist to restore the functionality. For example, there are some prostheses for functional or cosmetic use. There have been many studies on functional prostheses controlled by the patients. On the other hand, sensory feedback from prostheses is a recent biomedical research area to complement to motor function of those devices. There are two main techniques to provide sensory feedback: mechanical stimulation and electrical stimulation.

Functional electrical stimulation (FES) focuses on the regulation of activity in neurons by electrical stimulation. There are some implementations of FES devices on peripheral nervous system. These devices can restore the functionality of neuromuscular junction as well as sensation [2, 3, 4, 5]. To evoke sensation, the subjects' peripheral nerves are stimulated electrically in order to feed the captured information about the environment via sensors. It was shown that the subjects could sense some features such as vibration, pressure and proprioception. The evoked sensation can be controlled by changing parameters of the electrical stimulation. Varying specifications of stimulation provide different sensations and perceptive fields. It was also shown that the sensory feedback from the prosthetic robot arms provide better control of the device [2, 3, 5],and the stimulation of the sensory fibers reduces the phantom limb pain [6].

Some of these studies also showed that there are limitations on the stimulation parameters. For example, Raspopovic et al. [4] used the stimulation amplitude for intensity coding in the nerves and they also defined a 'pain threshold' level at which the stimulation amplitude caused pain sensation. Additionally, it was shown by Tan et al. [2] that increasing the charge delivered by the stimulation can activate different somatosensory sub-modalities.

When the benefits are considered, these prosthetics are very promising. On the other hand, the limitations should not be overlooked. While the amplitude of stimulation provides some information to the patient, high levels may cause annoying sensations (itching, burning, pricking pain, paresthesia) [2, 7]. Therefore, preventing these unwanted sensations may be a significant improvement of sensory neural prostheses.

1.2 Objectives

The main purpose of this thesis is to block unwanted sensations in somatosensory nerves by blocking the propagation of neural impulses in C fibers. For this purpose a hyperpolarizing DC stimulus is applied within a specific time window which does not overlap with the propagation of impulses from myelinated fibers.

1.3 Outline

The thesis is organized in the order of chapters. In Chapter 2 background information is given. The chapter starts with basics about the nerve cell and the action potential. Then, the functional electrical stimulation is introduced before giving the information about techniques for conduction block. The chapter is concluded with an overview of recent peripheral neuroprosthetics and peripheral nerve electrodes. In

Chapter 3, the experimental setup and the procedure are explained. The stimulation and blocking parameters are defined. The results are given in Chapter 4 in a similar organization as in Chapter 3. Lastly, in Chapter 5, the results are interpreted. Similarities and inconsistencies with the literature are discussed. The limitations of the electrode design, the procedure and those related with the physiological properties of the nerve fibers are presented. This chapter and thesis completed with possible improvements and successions for future work.

2. THEORY

Nervous system is one of the excitable tissues and it is the main processing system of the body. It collects data form environment via sensors and then process them. The output of the system is a behavior which can be a motor action like motion or homeostatic adjustments or cognitive state change [8].

The nervous system consists of the central nervous system (CNS) and the peripheral nervous system (PNS)(Figure 2.1). Brain and spinal cord constitute the CNS. The PNS is divided into two components: Autonomic and Somatic nerves. The autonomic system causes physiological changes to prepare the body for condition such as "fight or light" or relax. These changes include sweating, heart rate, blood pressure, and so on. The enteric system regulates the gastrointestinal tract, pancreas and bladder in cooperation with the CNS. Somatic nerves include sensory neurons which collect sensory input from the environment and the body. Additionally, PNS includes the motor nerves connecting to the voluntary muscles [8, 9, 10]

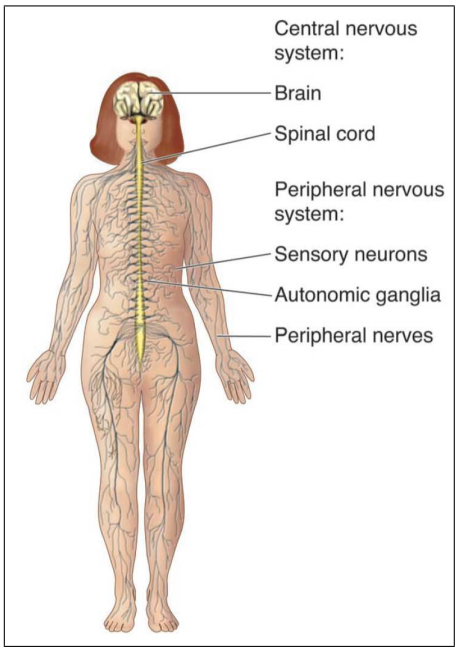

Figure 2.1 Central and peripheral nervous system [10].

2.1 Structure of The Nerve Cell

A nerve cell, i.e. a neuron is the main information processing cell of the nerves system. The neurons are excitable cells which transmit and modify impulse. A generic nerve cell consists of a soma and two types of process: the axon and dendrites. The soma (cell body) contains the nuclei and maintains the cell. The neuron receives the afferent signals via dendrites. The signal is summed along the membrane up to axon hillock where the axon arise. If the signal exceeds a certain potential, an action potential is generated. The axon transmits the efferent signals to the muscles, glands or neurons. The axon generally has collateral branches to send the signal to many end points. Axons may be surrounded by Schwann cells in the PNS so the membrane continues as the axolemma. The Schwann cells makes multiple turns around the axon and constitutes myelin sheath to insulate the axon membrane from the ion flows.

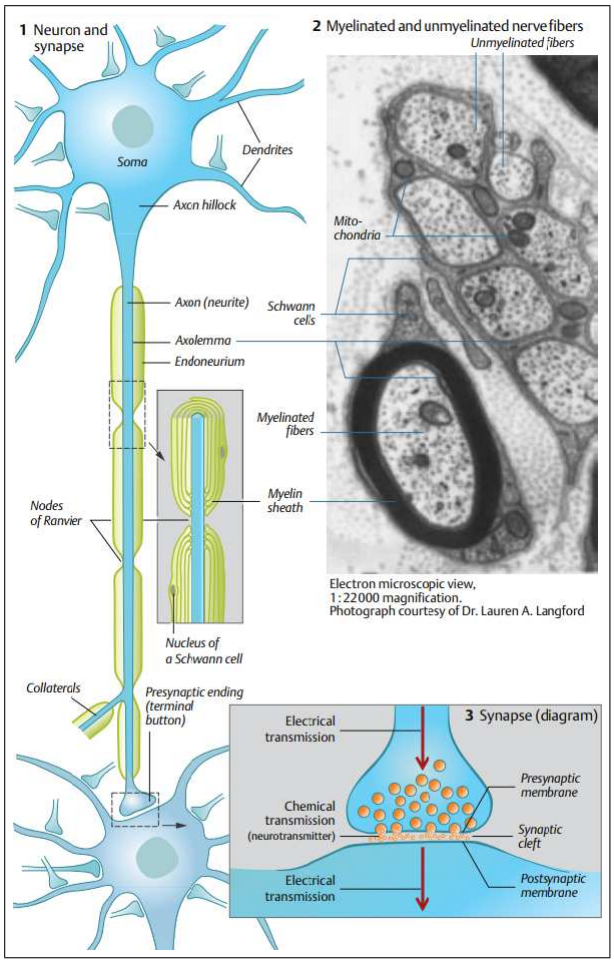

Figure 2.2 A generic nerve cell [11].

The myelin sheath is interrupted at nodes of Ranvier between two Schwann cells. This structure enables the axon to conduct signals faster in comparison with the unmyelinated axons. The axonal part is also called nerve fiber. The signal at the end of the axon is transmitted to the effectors through synaptic clef. The synaptic transmission is generally chemical. The neurotransmitters are packaged in vesicles and released to the synaptic cleft by exocytosis. The neurotransmitters released from the presynaptic membrane diffuse and reach the postsynaptic membrane where they bind to receptors which affect the membrane potential. According to the neurotransmitter type and the receptor, the transmission can be excitatory or inhibitory [11] (Figure 2.2).

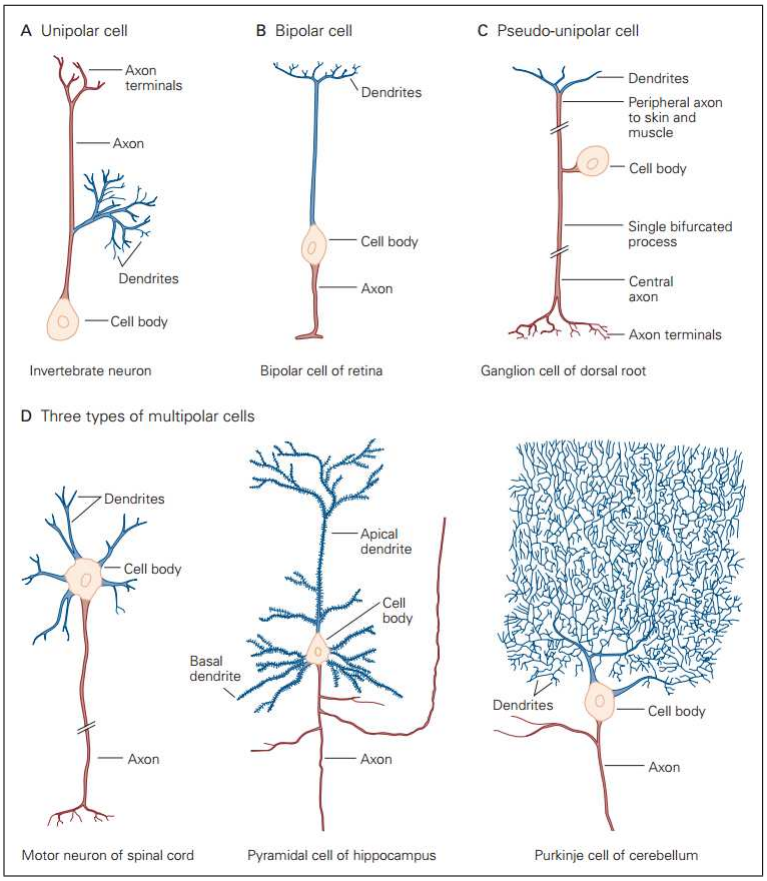

Figure 2.3 Neuron classification according to their connectional specificity [12].

The information flow through a neuron is from dendrite ends to the axonal ends. The motor neurons generally have the generic nerve structure with having soma in the spinal cord. On the hand, there are also different neuron types according to their

connectional specificity as demonstrated in Figure 2.3. The somatic sensory peripheral neurons are pseudo-unipolar cells. The somas of the motor neurons take place in the spinal cord while the sensory neurons have their soma in the dorsal root ganglia near the spinal cord. When we consider the human extremities, these nerves extend as bundles and make branches to innervate the end point.

2.2 Action Potential and Its Propagation

The nervous tissue is an excitable tissue. Neurons have a voltage difference between inside and outside due to the ionic concentration difference. The membrane of the cells prevents ions flowing freely. When a neuron is not active, in resting condition, it has around -60 to -70 mV difference with respect to the extracellular space. At resting potential it has more potassium in intracellular space, whereas sodium and chloride are concentrated higher in comparison to the intracellular space (Table 2.1). These concentrations are supplied by active transport mechanisms called Na-K pumps.

Table 2.1
Ionic concentrations across membrane at resting state [13].

Ion	Intracellular Concentration (mM)	Extracellular Concentration (mM)	Equilibrium Potential (mV)
K^+	400	20	-75
Na^+	50	440	55
Cl^-	52	560	-60

There are also voltage gated channels which let only specific ions flow across the membrane. At resting potential, part of the K^+ channels are open so the K^+ ions can flow while the Na^+ channels are mostly closed. The slight changes in states of these channels determine the resting potential. At resting potential there is balance between the chemical concentration gradient and the electrical gradient such that the total cur-

rent is zero. For example, a slight increase of Na^+ ion extracellular space results in influx of the ion because of the chemical concentration gradient increase pushing them in. On the other hand, this influx slightly depolarizes the nerve so the electrical potential changes to negative form the resting potential of the K^+. The change will be counteracted by the efflux of the K^+. As a result the Na^+ influx will be balanced with the K^+ outward flow. [13]

The membrane potential returns its resting potential when it slightly deviates from the rest. When the nerve is further depolarized, another phenomenon occurs: action potential (Figure 2.4). The critical voltage is called threshold where the action potential starts. The voltage gated Na^+ channels open and fast influx of Na^+ occurs due to the concentration gradient. This sudden positive ion inrush makes the intracellular space more positive up to 20-30 mV so the membrane is depolarized. The K ions efflux proceeds via voltage gated K+ channels which have slower opening rate. At the repolarization phase of the action potential, the Na^+ channels become inactive so the influx of positive ions stops. The K^+ channels are still open so the outward flow of positive ions becomes dominant and the membrane repolarizes. Because the K^+ channels have slower opening and closing rate, the membrane becomes more negative than the resting potential until the K channels close. This part is called after-hyperpolarization. Then the Na-K pumps restore the ionic concentration back to the resting conditions.

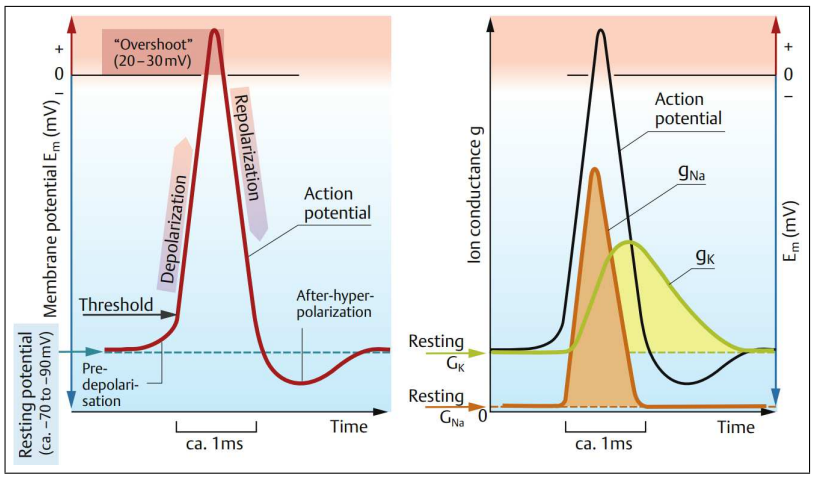

Figure 2.4 Action potential (left), and Na and K conductance of membrane (right) [11].

When we consider an axon, it looks like a cable. The membrane works like insulator and intracellular space is conductive. A depolarization at a point on the membrane raises the membrane potential to less negative values rapidly while the adjacent segments are still at resting potential. This potential gradient results in passive current flow from adjacent to depolarized region. As a consequence, the adjacent region will also be depolarized. When this depolarization passes the threshold, action potential starts at the adjacent region as well. So the action potential will propagate along the axon (Figure 2.5).

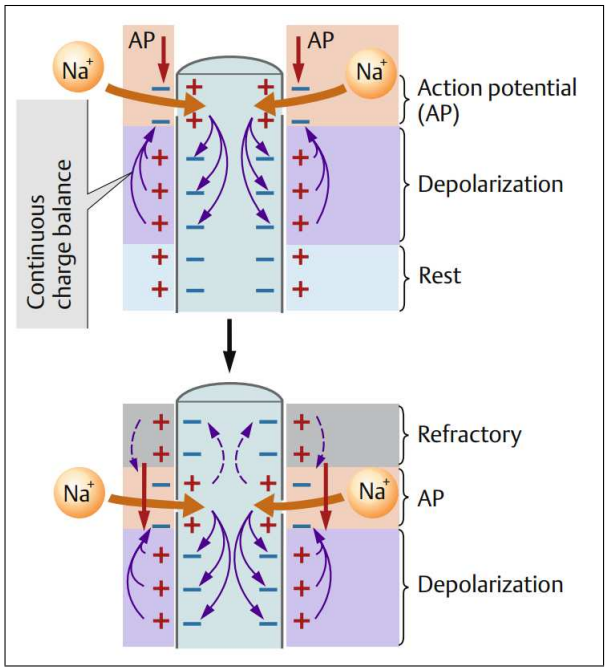

Figure 2.5 Action potential propagation [11].

The speed of the propagation is mainly determined by two factors which are fiber diameter and the myelination. According to the simplified nerve model, the nerve consists of passive electrical components. The membrane has capacitive (C_m) and resistive properties (R_m). The intracellular space has resistive (R_a) property. If a fiber is approximated to a cylinder, the membrane capacitance of infinitesimal length increases proportional to circumference of the cylinder ($2\pi \times radius$), and the membrane resistance depending on the number of ion channels decrease proportional to the radius, while the axoplasmic resistivity inversely proportional with square of the radius

($\pi \times radius^2$). The increase in the C_m slows down the voltage change in adjacent region because it requires more current flow to reach the threshold. The decrease in R_m counters this slowdown because the current can flow faster across the membrane so does the depolarization. The adjacent region is affected faster when the R_a decrease. Because the R_a inversely proportional to square of the diameter, it outweighs the others. Consequently, the larger diameter is, the faster the conduction is.

Myelination is more effective than the larger diameter. The mean conduction velocity of unmyelinated fibers is around 1 m/s whereas the myelin sheath speeds up the conduction up to 80 m/s. The Schwann cells wrap the segments of fiber tightly so that the fiber is isolated from the external space. The gaps between the Schwann cells called Ranvier nodes are exposed. The action potential propagates as if jumping between the nodes because the voltage gated channels concentrated mostly at the nodes and the action potential conducted passively through the myelinated parts. This type of propagation is called saltatory propagation and results in faster conduction (Figure 2.6). [11]

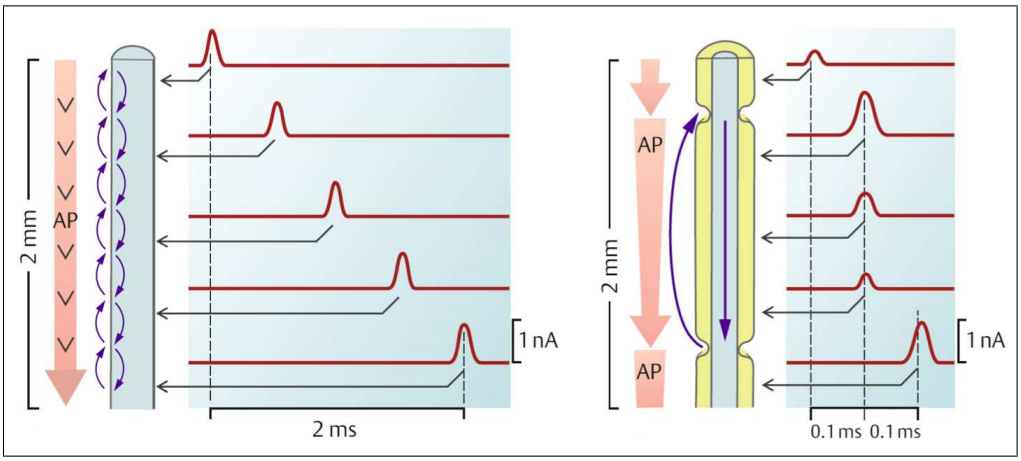

Figure 2.6 Propagation of current flow in unmyelinated fiber (left) and myelinated fiber (right) [11].

2.3 Electrical Stimulation

An action potential in a peripheral nerve can be initiated by synaptic transmission or sensory receptors in a living body. The chemical transmission is done by the neurotransmitters. The neurotransmitter is released by the presynaptic neuron and the

neurotransmitters bind receptors on the postsynaptic neuron. The receptors regulate the ion channels. If the transmission is excitatory, there is a local depolarization in the postsynaptic neuron. The local depolarization propagates passively and is summed at the axon hillock. If the sum exceeds the threshold, an action potential is initiated [11]. The sensory receptors can also initiate action potential. The sensory receptors can transform the stimuli energy into electrical signals. For example, pressure on the skin or stretch of a muscle can be detected by a specialized mechanoreceptor and the receptor changes the ion permeability of the nerve. The permeability determines the potential. If the receptor potential reaches the threshold, the action potential occurs [14].

Electrical stimulation by an external source can also change the membrane potential. If the current depolarizes the membrane up to threshold, the voltage-gated Na channels will be activated and action potential will be evoked. The membrane potential can also be hyperpolarized with electrical stimulation [15].

2.3.1 Pulse Stimulation and Compound Action Potential

An action potential is initiated in a nerve if the membrane potential is depolarized up to the threshold. In other words, at resting state the membrane potential is negative as the reference is extracellular space and an action potential occurs when this voltage becomes less negative up to the threshold. The membrane potential can be manipulated by an external source artificially.

In the case of stimulation with external electrodes whose cathode is close to the nerve membrane and anode is far away, the stimulation causes the current flow from intracellular space to out. As a consequence, the intracellular space becomes less negative with respect to outside so the membrane depolarizes. In Figure 2.7, the anode electrode is positioned close to the nerve and the cathode is positioned far away. The stimulation current flows in to the nerve under the electrode and hyperpolarizes the nerve [16]. When the stimulation polarity is reversed (cathode), the direction of current flow and the polarization of the nerve will reverse.

The amount of delivered charge determines whether the depolarization is

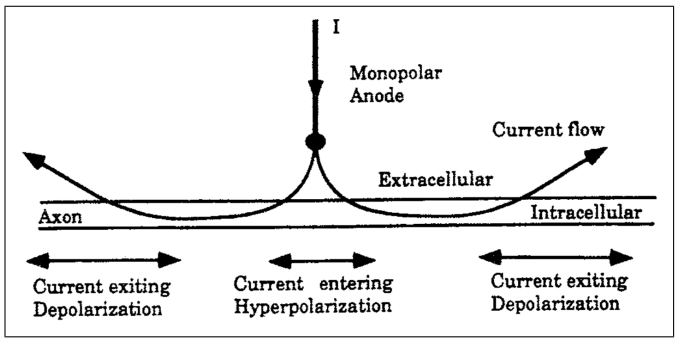

Figure 2.7 Current flow with anodal stimulation [16].

enough to excite the nerve. Thus, the amount of charge required to reach the threshold can be induced with a long duration and low amplitude or short duration and high amplitude. On the other hand, even if infinitely long stimulation is applied lower than certain amplitude, it cannot evoke action potential. The lowest amplitude to evoke action potential is called rheobase. When the minimum amplitudes required to stimulate the nerve with different durations are plotted, the strength-duration curve is obtained [17]. When the amplitude of stimulation is doubled the rheobase, the required duration for threshold is called chronaxie which defines the most energy efficient stimulation in respect to injected charge (Figure 2.8).

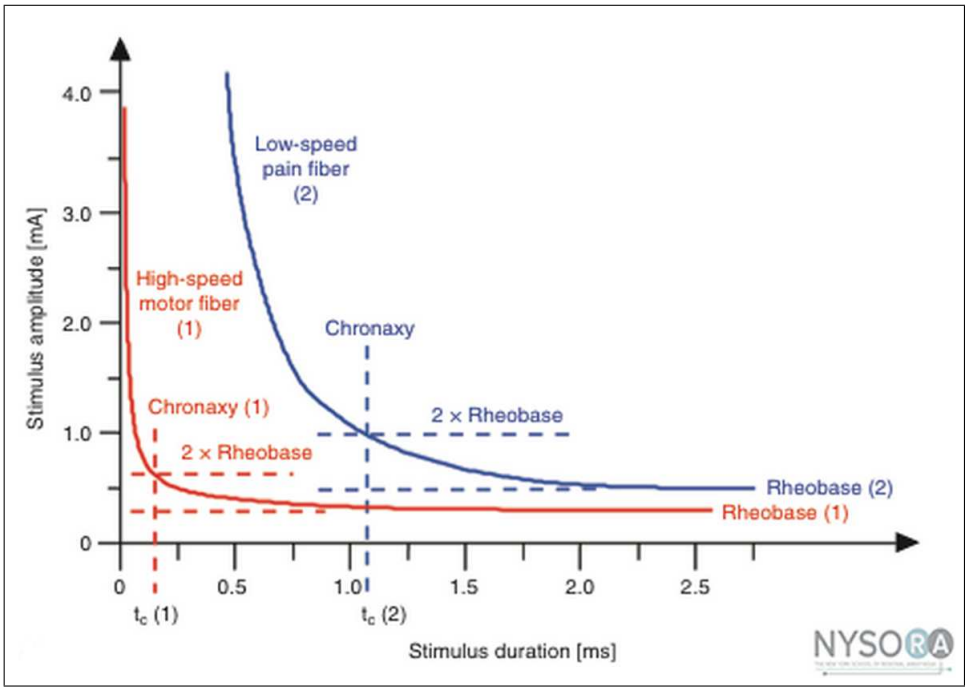

Figure 2.8 Strength duration curve of two different nerves [18].

When we consider a bundle of nerve, there are many fibers with different properties such as diameter and myelination, so they have different conduction velocities. They can be classified according to this parameters (Table 2.2).

Table 2.2
Classification of somatic peripheral nerve fibers according to the conduction velocity [19].

	Muscle nerve	Cutaneous nerve[2]	Fiber diameter (µm)	Conduction velocity (m/s)
Myelinated				
Large diameter	I	Aα	12–20	72–120
Medium diameter	II	Aβ	6–12	36–72
Small diameter	III	Aδ	1–6	4–36
Unmyelinated	IV	C	0.2–1.5	0.4–2.0

A fibers are myelinated and C fibers are unmyelinated. The C fibers have the slowest conduction. A fibers have also subgroups called alpha, beta and theta. The Aα fibers have largest diameters and the largest myelination and Aβ and Aδ have smaller, respectively. In each subclass there is a range of conduction velocities (Figure 2.9).

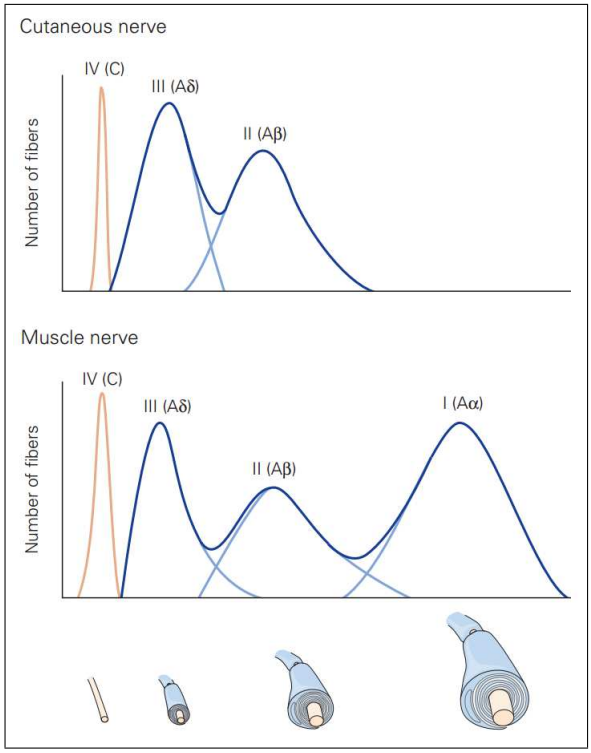

Figure 2.9 Distribution of nerve classes in peripheral nerve. x axis is velocity [19].

Each class also shares common functionality. They innervate special end points. Within the sensory nerves, the fastest ones make synapses with muscle while the slowest ones relay nociception. Their general functions and innervating receptors are given in Table 2.3.

Table 2.3
Receptor types and innervating fiber classes and modalities [19].

Receptor type	Fiber group[1]	Fiber name	Modality
Cutaneous and subcutaneous mechanoreceptors			Touch
Meissner corpuscle	Aα,β	RA1	Stroking, flutter
Merkel disk receptor	Aα,β	SA1	Pressure, texture
Pacinian corpuscle[2]	Aα,β	RA2	Vibration
Ruffini ending	Aα,β	SA2	Skin stretch
Hair-tylotrich, hair-guard	Aα,β	G1, G2	Stroking, fluttering
Hair-down	Aδ	D	Light stroking
Field	Aα,β	F	Skin stretch
C mechanoreceptor	C		Stroking, erotic touch
Thermal receptors			Temperature
Cool receptors	Aδ	III	Skin cooling (<25°C [77°F])
Warm receptors	C	IV	Skin warming (>35°C [95°F])
Heat nociceptors	Aδ	III	Hot temperature (>45°C [113°F])
Cold nociceptors	C	IV	Cold temperature (<5°C [41°F])
Nociceptors			Pain
Mechanical	Aδ	III	Sharp, pricking pain
Thermal-mechanical (heat)	Aδ	III	Burning pain
Thermal-mechanical (cold)	C	IV	Freezing pain
Polymodal	C	IV	Slow, burning pain
Muscle and skeletal mechanoreceptors			Limb proprioception
Muscle spindle primary	Aα	Ia	Muscle length and speed
Muscle spindle secondary	Aβ	II	Muscle stretch
Golgi tendon organ	Aα	Ib	Muscle contraction
Joint capsule receptors	Aβ	II	Joint angle
Stretch-sensitive free endings	Aδ	III	Excess stretch or force

Mechanoreceptors sense the physical deformation in the tissue. The skin has 8 types of receptor. Merkel cells and Ruffini endings are innervated by slowly adapting fibers which respond by continuous firing to steady stimulation. Merkel cells (SA1) signal the amount of pressure on the skin so they are important for perception of edges, corners, points, and texture. The Ruffini endings (SA2) are more sensitive to skin stretch so they are important for sensing shape of objects besides movement of fingers. Meissner and Pacinian corpuscles are innervated by rapidly adapting fibers which respond to vibrations in the skin but not to steady pressure. Meissner corpuscles (RA1) play an important role in the initial touch with objects, for texture perception and low frequency vibrations. Pacinian corpuscles (RA2) are sensitive to very small deflections

and high frequency vibrations. The hair receptors are sensitive to hair motions but not to steady pressure. C mechanoreceptor have low threshold for skin movement and are thought to be important for affective touch.

Muscle and skeletal mechanorecptors play important role in proprioception, i.e. movement and body position. Muscle spindle sense muscle length and therefore, provide information about amplitude and speed of muscle movements. The Golgi tendon organs measure the force exerted by the muscle on to the tendon. Joint capsule receptors provide information about joint position.

In the skin, there are also nociceptors responding to mechanical stimuli, thermal, and chemical causing pain. The sensations are related pain sensation. The mechanosensitive nociceptors cause sharp and pricking pain. The heat sensitive ones provide burning or freezing pain. The polymodal nociceptors sense noxious mechanical and temperature stimuli and also irritant chemicals. There are four types of thermal receptors which are activated depending on the deviation form skin surface temperature.

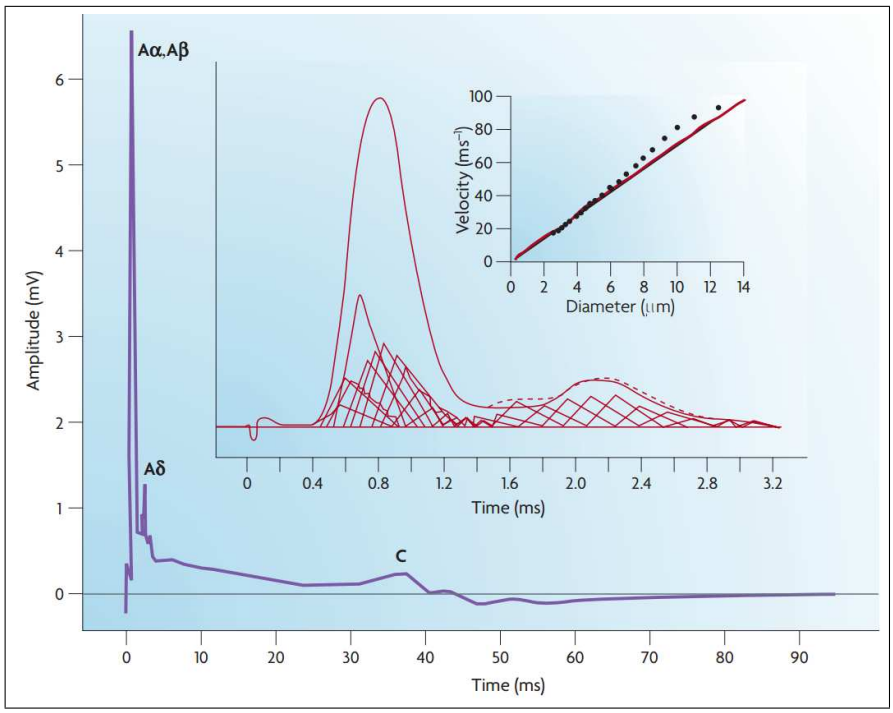

Figure 2.10 CAP example. The purple trace is a CAP of mammalian saphenous nerve (37 mm distance between recording and stimulation side). A fibers spread less and have shorter latency than the C component. The inset with red curves depicts the summation of A fibers' action potentials represented as triangles. Top right graph shows the relationship between fiber diameter and conduction velocity [20].

The activity in a peripheral nerve bundle can be recorded extracellularly. The record will have different shape than an action potential because the record is sum of the action potentials of many fibers. This type of recording shows a compound action potential (CAP). When the bundle is stimulated at a point with suprathreshold stimulation, the recording at a location away from the stimulation has specific components based on distribution of conduction speeds. As shown in Figure 2.10, A fiber subgroups generate high peaks with short latencies, C fiber group generates small peak with long latency.

In addition, the fibers with different properties in a nerve bundle have different thresholds so the change in stimulation parameters causes excitation in only some of the fibers. The fibers with larger diameter are recruited before the smaller ones by increasing stimulation strength [13].As shown in Figure 2.11, the increasing stimulation strength partially excites Aα component and then recruits all Aα fibers therefore there is no further increase in the Aα component. However, increasing stimulation strength recruits additional fibers and generates other components in the CAP response.

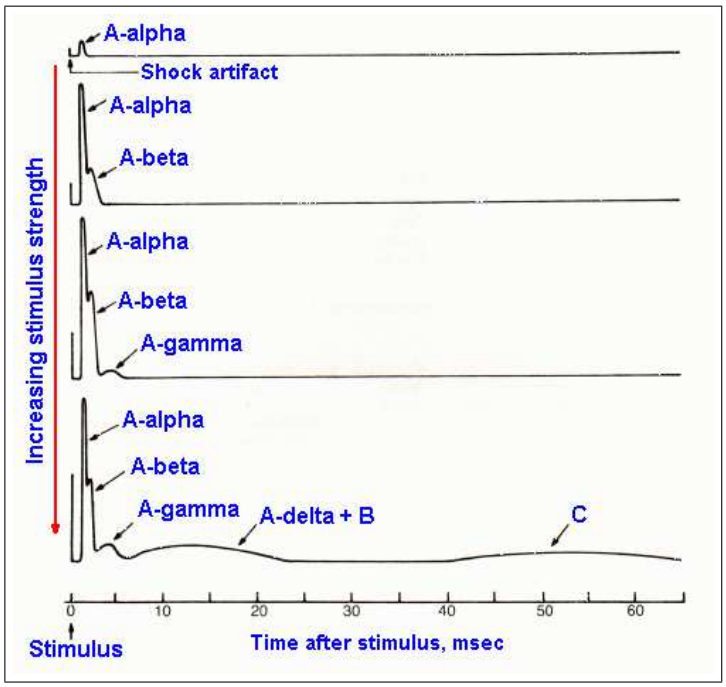

Figure 2.11 Sample recordings from the sciatic nerve with increasing stimulation amplitude. (The electrical stimuli applied to the nerve away from stimulation side 80 mm away) [21].

2.3.2 Hyperpolarization

Once the action potential starts propagating, it cannot reverse direction because of after hyperpolarization. While propagating, the action potential leaves behind hyperpolarized region where the slow K channels polarize the membrane slightly below the resting potential. So the injected current by the action potential to the proximity is not enough to depolarize the opposite direction up to the threshold [13].

In the case of the artificial electrical stimulation, if the stimulation is applied somewhere along nerve fiber, the initiated action potential propagates both direction because the membrane is at the resting potential. In other words, there is no hyperpolarized region around the action potential to prevent the propagation. Once the action potentials are initiated, they leave hyperpolarized region behind them so both action potentials will not change their propagation direction.

The cathodic extracellular stimulation injects negative charge to extracellular space so membrane potential becomes less negative and action potential occurs. In contrast, the anodic extracellular stimulation draws negative charge from the extracellular space so the membrane is hyperpolarized. As a result, when a propagating action potential reaches this region, the action potential cannot depolarize the membrane up to the threshold and it is blocked.

2.3.3 Conduction Blocking

The conduction in a nerve fiber can be blocked with different techniques. Blocking the voltage gated ion channels with chemicals is one of them. Tetrodotoxin binds to the Na channels and prevents the Na^+ flow. Tetraethylammonium binds to the voltage-gated K channels and affects the permeability. But these chemicals are not selective to the fiber types [22]. There are also chemicals which can block the fiber types selectively such as capsaicin blocks unmyelinated fibers selectively [23]. But chemicals lose effectiveness in time so they must be applied repetitively.

Electrical stimulation is also utilized for blocking conduction. The parameters of the stimulation can be adjusted for different blocking purposes. The block can be

achieved instantaneously and the recovery of the nerve from the block is also very fast without irreversible damage with proper parameters.

2.3.3.1 DC Blocking. Some of the blocking techniques utilize the monophasic stimulation. The polarity, duration and amplitude are main parameters to control. The waveform of the stimulation is another parameter. There are varieties of the wave shape such as rectangle, triangle, triangle with unequal rise up and fall durations, and exponential rise up or decaying fall.

Block of action potential can be achieved by collision method. In this method, action potential is stopped by collision with another action potential propagating in opposite direction [24]. For example, an action potential propagating orthodromicly can be blocked by colliding with an artificially evoked antidromic action potential. But the blocking stimulation itself also evokes an orthodromic action potential [25].

Another technique enables the selective activations of the nerve by bipolar electrode design. Nerve is activated at the cathode and the anode is used as blocking electrode. In other words, the electrode configuration enables blocking action potential generated by stimulating pulse. The principle in this technique is that the cathode evokes action potential and the action potentials in larger fibers reach the anode first and are blocked. The stimulation is turned off before the slow ones reach the anode, so they pass [26].

In addition, anodal blocking is also possible. The simulations show that under the anode electrode the nerve is hyperpolarized. This hyperpolarization is adequate so that the arriving action potential cannot depolarize the region up to threshold. Thus, when the propagating action potential reaches the hyperpolarized region the conduction is blocked (Figure 2.12) [26, 27]. But this blocking technique has a drawback that the termination of the stimulation may cause an excitation (anodal break excitation). The break excitation can be eliminated by slowly turning off the blocking stimulation with exponential decay(Figure 2.13) [28, 29, 30].

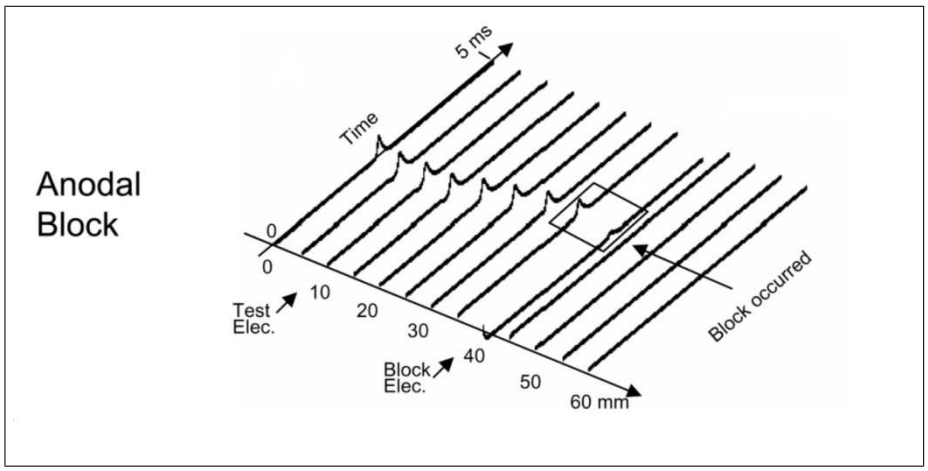

Figure 2.12 Anodal block (simulation). The anode was positioned at 40 mm and the action evoked at 10 mm [27].

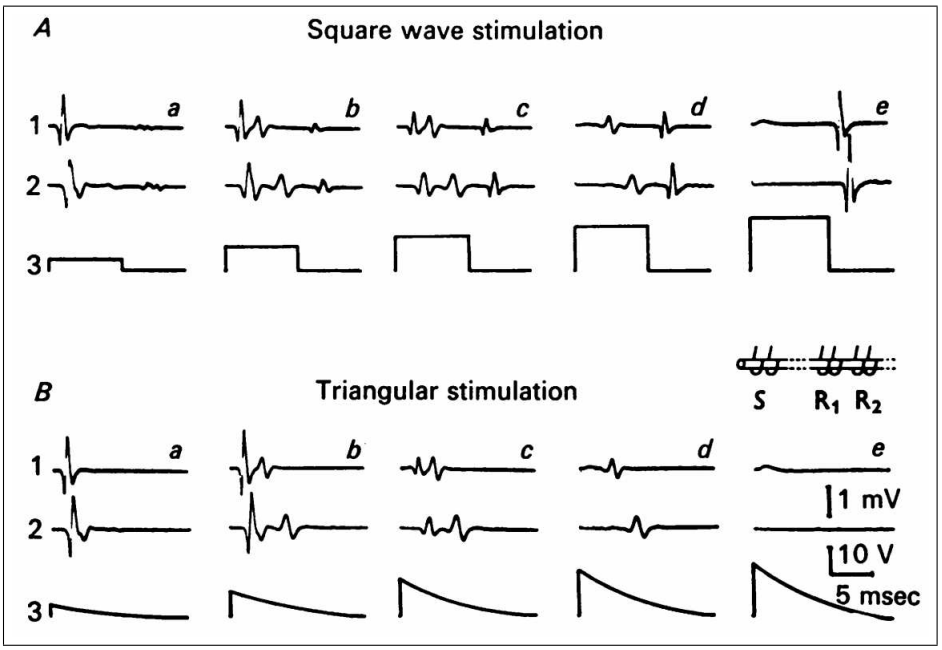

Figure 2.13 Effect of exponential decay. The stimulation is applied through electrode S. The traces numbered 1 and 2 are compound action potentials from R_1 and R_2. The traces numbered 3 are stimulation. A: Square pulse to block. B: No break excitation with decay offset [28].

An external stimulation draws or injects charge to the extracellular space. While this charge causes main change underneath the electrode, it also has effect on proximity. For example, a cathodic stimulation depolarizes the nerve right under the electrode. The local depolarization also withdraws current from close proximity in the axoplasm. As a result, the proximity of electrode is hyperpolarized while the region under it is depolarized. This effect is called virtual anode. The same phenomenon also happens

with anodal stimulation and is called virtual cathode(Figure 2.14). If this virtual cathode effect reaches to the threshold level, an action potential will be evoked.

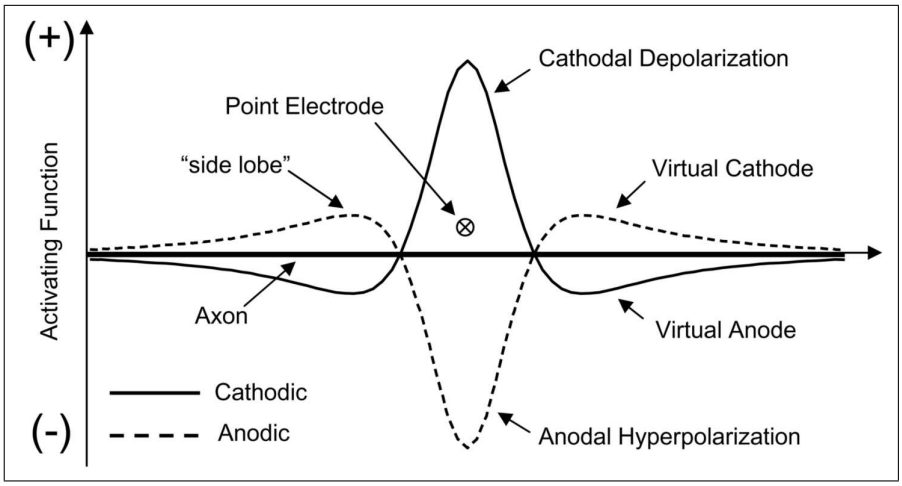

Figure 2.14 Virtual cathode and virtual anode effects [27].

In these simulations mentioned above, the electrode is modeled as monopolar point source. This means that the stimulating electrode is infinitesimally small and the return electrode is placed at infinity. But this is not the case in practical applications. Cuff electrodes are commonly used in functional electrical stimulation and the electrodes are placed close to nerve. The bipolar electrode designs also have virtual anode and cathode effect. But the tripolar designs significantly reduce this effect. A cathode lead is placed with equal distance between two anodic leads (Figure 2.15) [25, 26, 31, 32, 33].

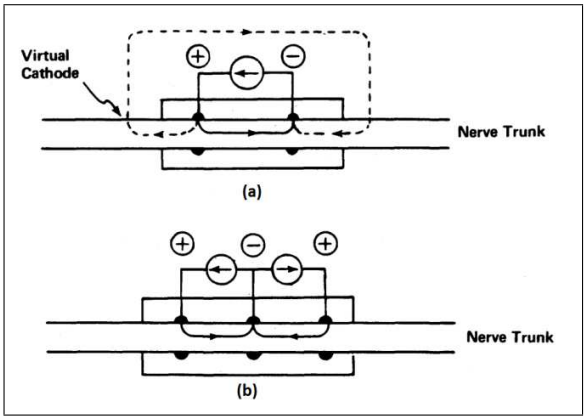

Figure 2.15 Current flow between electrode leads a) bipolar b) tripolar design [25].

2.3.3.2 AC Blocking. The conduction block is also achievable with alternating current. The charges during positive and negative phases are balanced in this type of stimulation. The stimulation of the motor nerve at low frequencies can create a fatigue in the muscle so additional action potential through the motor fibers becomes irrelevant. As a result, the block is achieved at muscle level [34]. On the other hand, at kilohertz frequencies, the conduction is blocked at the nerve fiber. To block the conduction in myelinated fibers, the nerves with smaller diameter require higher amplitude of stimulation and the increasing frequency also requires higher amplitudes (Figure 2.16) [35].

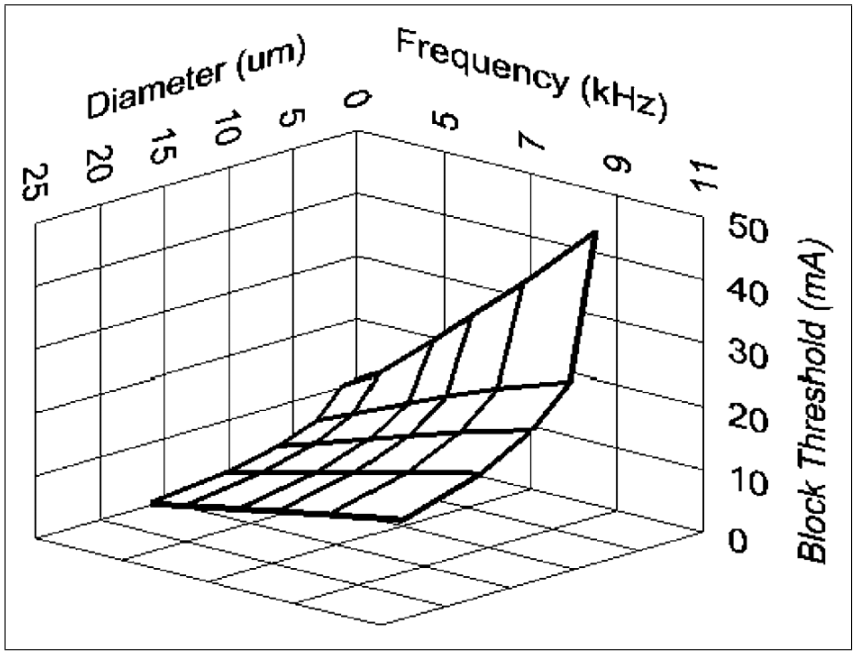

Figure 2.16 The change in block threshold with respect to fiber diameter and stimulation frequency[35].

The block threshold has a monotonic increase with increasing frequencies for myelinated fibers. Whereas the unmyelinated fibers has an increasing and then decreasing trend in block threshold with increasing frequency [36].

The underlying mechanism is not certain in AC blocking. There are three possible explanations. First, the stimulation causes excessive accumulation of extracellular potassium [37]. Secondly, the simulation using the Hodgkin-Huxley (squid axon model) and Frankenhauser-Huxley (frog axon model) assumes that outward potassium

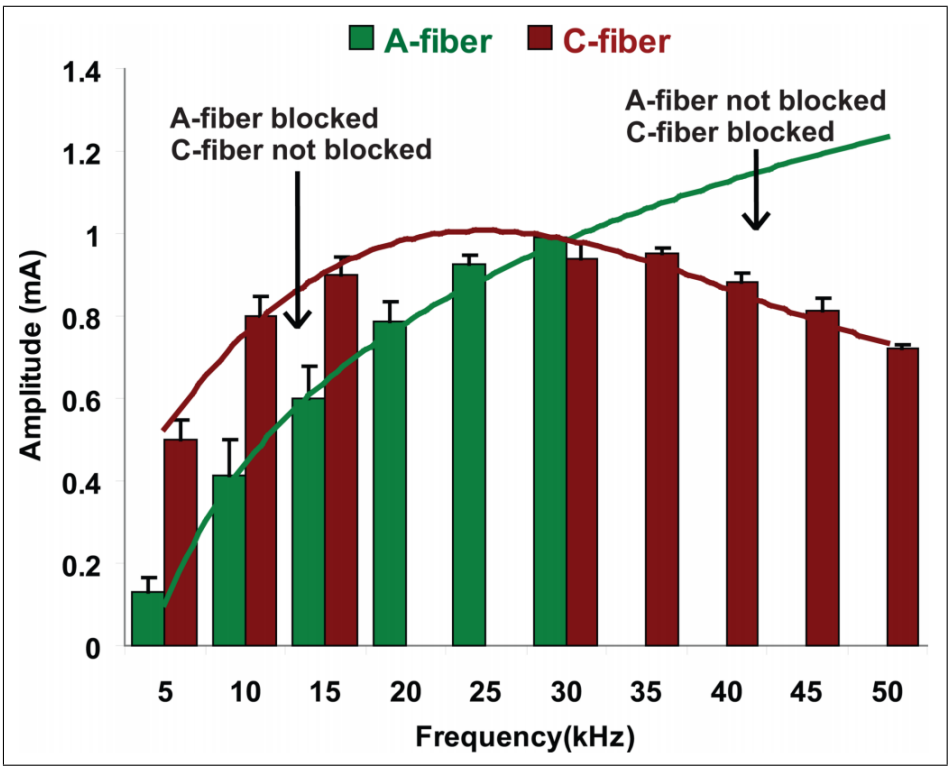

Figure 2.17 Change of block threshold amplitudes with frequency change for A fibers and C fibers[36].

currents overwhelm the inward sodium currents [35, 38, 39]. The third view assumes that the sodium channel inactivation causes the block [40, 41, 42].

2.3.3.3 Advantages and Disadvantages of DC Blocking. Electrical stimulation provides an effective manipulation of nerve activity. It has instantaneous effect and the nerve recovery is fast when the stimulation is turned off. On the other hand chemical stimulation requires some time to affect and recovery also takes time.

The unbalanced stimulation has more destructive effect than the balanced one [43, 44]. But there will be asynchronous firings at onset of the AC blocking stimulation inevitably. The ramped onset is proposed to reduce the onset firings but this worsens the situation. In contrary, the high frequency and high amplitude stimulation reduces the onset asynchronous firing [45]. Another approach is the combination of AC and DC blocking. In this approach, there are two blocking sides along the nerve. The AC blocking side is closer to the stimulation and the DC blocking side proceeds along

the propagation direction. The conduction is blocked by the AC stimulation and the asynchronous firings due to the onset of AC stimulation are blocked by the DC hyperpolarizing block. When the asynchronous phase overs, the DC blocking stimulation is turned off [46].

In practical applications, the energy consumption of such AC blocking device and the asynchronous firing and the amount of the charge to the tissue by the stimulation is another critical issue. The approach to reduce them is that the stimulation starts with high frequency and high amplitude then transition to the lower amplitude and lower frequency. The AC blocking causes less asynchronous firings when it starts with high frequency while the blocking threshold is higher for high frequency. Once the asynchronous firing ceases the stimulation amplitude and frequency can be reduced [47].

Hyperpolarizing DC block has advantages of instantaneous effect without onset firing over AC blocking. One of the drawbacks is the anodal break excitation. The hyperpolarization causes the potassium ions to flow out so when the stimulus is ceased, the membrane becomes depolarized and this depolarization can be up to threshold level. On the other hand, instead of instantaneous turn off, a decaying cessation of the stimulus can eliminate the break excitation [28, 29].

2.4 Structure of Frog Sciatic Nerve

Frogs are commonly used in nerve studies. The first myelinated nerve model was driven from frog nerve [48]. Sciatic nerve is commonly used for extracellular stimulation and extracellular recording. The neuromuscular complex also provides valuable information for myelinated nerve studies.

The electronmicroscopy studies show that the sciatic nerve contains 1163 myelinated and 1281 unmyelinated fibers and a brachial nerve has 802 myelinated and 857 unmyelinated fibers (*Triturus viridescens*).There is an approx. 1:1 ratio between the number of myelinated and unmyelinated fibers. Unmyelinated fibers occupy less than 3% of neuroplasm in the peripheral nerve. The average crosssection areas are 31.48

μm^2 and 0.89 μm^2 for myelinated and unmyelinated fibers, respectively [49]. The internodal length is formulated as $L = 146 \times D$ (D: diameter μm). Frogs have all fiber types such as A fiber subgroups and B and C fibers [50].The ratio of axolemma diameter to total diameter for myelinated fiber is 0.7. When the conduction velocity of A fiber vs diameter is plotted, the fitted line has a slope of 2 (m/s)/μm [51]. The average conduction velocities of different fiber types are reported as Aα 21 m/s, Aδ 2 m/s and C 0.3 m/s [52] and in another source A fibers 40-7 m/s, C fibers 0.3-0.6 m/s [53].

2.4.1 Similarities and Differences Between Mammalian and Frog Sciatic Nerve

The sciatic nerve of frog is commonly used in studies of nerve stimulation. Both mammals and frogs have similar classes of fibers such as myelinated A fibers and autonomic B fibers and unmyelinated C fibers with variations in their properties. However, both mammals and frogs have approximately 1:1 ratio between the numbers of myelinated fibers and unmyelinated sensory fibers [54].

The main difference between mammalian and frog nerve is the fascicular structure of the nerve. The peripheral nerves of mammals are grouped in fascicles surrounded by connective tissue. The number of fascicles changes as the nerve branches. Mammalian peripheral nerve bundles have three layers of supportive tissue, epineurium, perineurium, and endoneurium. The epineurium is the outermost layer. It carries blood vessels to supply the nerves. The perineurium constitutes the fascicular structure and provides tensile strength. The endoneurium composes the extracellular matrix of the axons [55]. However, the frog does not have a clear epineurium which is unsubstantial fragments where blood vessels lie. However, perineurium surrounds all the fibers as bundle without fascicles and it does not have lamellated structure like mammals (Figure 2.18). The endoneurium is less obvious in comparison to mammalian nerve [56].

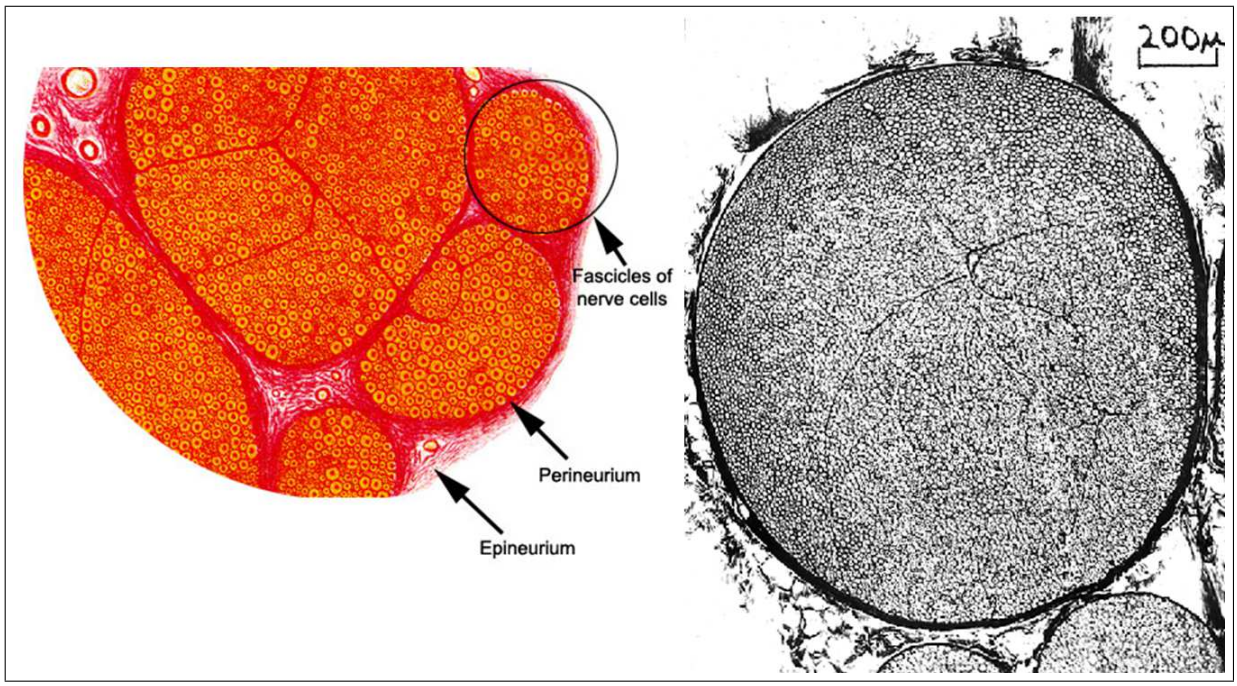

Figure 2.18 Fascicular structure of mammalian nerve(left), nonfascicular structure of frog nerve bundle (right) [57].

2.5 Peripheral Neuroprosthetics

There are patients who have neural problems. These problems may result from diseases, neuropathies, damages at different level of the nervous system such as brain stroke, spinal injuries or lose of extremities. The neuroprosthetics aim to reduce the dysfunctionality, and substitute the missing function.

There are many neuroprosthesis studies focusing on functional electrical stimulation (FES) of peripheral nervous system. Some of these have been used in practice. These include respiratory pacing [58, 59], control of pain [60, 61, 62], control of defecation and urinary incontinence [63, 64], activation lower extremities motion [65, 66, 67, 68, 69], control of hand movements [70, 71, 72].

These prosthetics require an interface to stimulate the nerve and to record from it. Different microelectrodes have been developed which are mostly invasive at different invasiveness level. The more invasive electrodes generally provide better selectivity. However, all of them need to be safe regarding electrical stimulation and biocompatibility. The peripheral electrodes can be grouped according to their level of invasiveness.

For example, surface electrodes are generally used for recording EEG, EMG, and ECG are noninvasive. Extraneural electrodes are placed around epineurium may be considered as minimally invasive. For example, the epineurial (Figure 2.19a) and helical electrodes (Figure 2.19b) are sutured to the epineurium. Epineurial electrodes are used in FES applications for breathing control, foot-drop improvement and neuropathic pain relief. Helical electrodes, placed around of the nerve, can be used for therapeutic applications. Book electrodes are commonly used in clinic for urinary bladder management. Cuff electrodes (Figure 2.19d) have an insulation tube encircling the nerve so the stimulating current is confined to the inner space of the electrode and the stimulation does not affect the surrounding tissue. The tripolar (cathode in the center between two anodes) design reduces the current leakage out of the cuff. They provide long term stimulation and recording. Flat-interface nerve electrodes (FINE) (Figure 2.19f) are the reshaped version of cuff electrode. By flattening the nerve into a more elliptical shape, the inner fibers of the nerve bundle become more accessible and the surface area increases so the stimulation penetrates better. Interfascicular electrodes (Figure 2.19e) are more invasive. They are places in the particular way in the nerve in order to provide better selectivity. Longitudinally implanted intrafascicular electrodes (LIFE) have an exposed area on a longitudinal conductive wire which inserted in the fascicle. This design enables higher signal to noise ratio and more selective recruitment. Regenerative electrodes (Figure 2.19c) provide an interface with a high number of fibers. This electrode has an array of holes and is placed between the stumps of a severed peripheral nerve. Therefore this design is the most invasive one which is typically used in the most difficult applications. The nerve grows through the holes and eventually each hole enables an interface to very small number of fibers [55].

Considerable scientific and technological efforts have been devoted to develop neuroprostheses and hybrid bionic systems that link the human nervous system with electronics, with the main aim of restoring motor and sensory functions in disabled patients. There are prostheses that patients can control to move a robotic device by recording EMG activity or nerve activity. However, the patients have to follow the device visually, because there is no somatosensory feedback about the movement. On the contrary, the function of the normal hand strictly depends on the proprioceptive feedback to control the movement and tactile feedback for fine discrimination so sen-

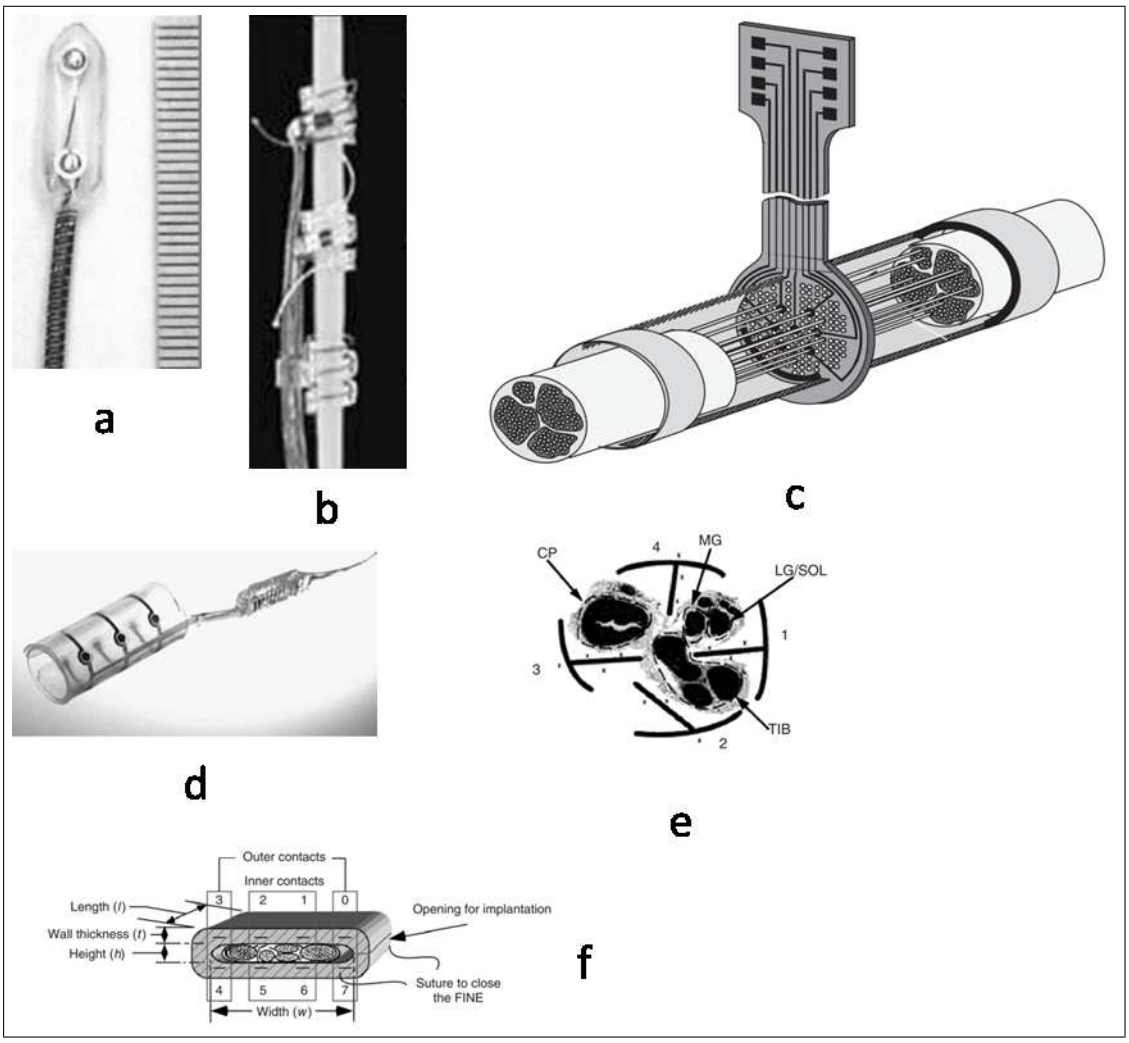

Figure 2.19 Some electrode designs for interface with peripheral nerve a) epineurial b)helicoid c) regenerative d) cuff e) interfascicular f) FINE [55].

sory feedback form the prosthesis can improve the control performance. There are prostheses that the feedback is provided by stimulation of the somatosensory afferents.

Electrical stimulation of the rapidly adaptive type 1 fibers evokes tactile sensations of flutter and the rapidly adaptive type 2 evokes those of vibration. The stimulation of the slowly adapting type 1 causes sensation of constant pressure, whereas slowly adapting type 2 evokes skin stretch and joint movement. In the study of Macefield et al. [7],they used microelectrodes which is positioned to medial or ulnar intrafascicles of the hand of thirteen subjects. The electrodes were used both the recording of single fiber and stimulation. They used the recordings to identify the fiber type. The joint afferents were identified with the following criteria: not responding to the cutaneous stimulation, not responding to the pressure on the muscle, and responding to high

pressure on the joint and extreme rotation of the joint. The fibers innervating the muscles were identified by pressure on muscle or stretch of muscle. The cutaneous nerves were identified as SAI and RAI afferents which have smaller receptive field, and SAII and RAII, which have larger receptive field. Additionally, SAII responds the skin stretch while SAI does not. They identified 65 afferents which were 11 joint afferents, 19 muscle afferents, and 35 cutaneous. They used 0.3-1.24 V constant voltage or 0.4-13 μA biphasic current pulses with 0.1-0.2 ms duration at 1-100 Hz. The stimuli were delivered as single pulse or a pulse train lasting 0.5-2 s. The stimulation amplitude was increased until the subject perceived the stimulus. The stimulation of 8 the joint afferents were perceived by the subjects. A single pulse was perceived as a deep punctate pressure at the joint and train of pulses were perceived as movement. As the frequency of the stimulation was increased, the extent of the perceived movement was increased. However, the perceived movement was not close to the limits of joint. In addition, the subjects felt slight movement by stimulation of muscle afferents. However, only two muscle afferents of 19 could be stimulated without causing muscle activation so the authors speculated that the perception due to the stimulation of the 17 fibers resulted from slight skin deflection. 9 of the cutaneous fibers were classified as RAI, 8 of them were SAI, and 8 of them were SAII. 88% of the RA fibers generated sensation of tapping which developed into flutter and then to vibration or tingling as the stimulation frequency increased from 20 to 100 Hz. The stimulation of SAI caused sustained pressure whose intensity increased with increasing stimulation frequency (10-80 Hz). 15 of 18 SAII fibers evoked some tactile sensation or mild painful sensation.

Amputation of an extremity causes changes in sensorymotor pathways. Furthermore, atrophic changes occur in the nerves. Dhillon et al. [5] showed that short-term training enables the amputees to restore some functionality. In their study, they used LIFE electrodes to provide interaction between long term amputees (n=13, amputee for average 7.3 years) and an electrical device. The electrodes were used for feedback of touch/pressure and joint position, besides recording from the motor fibers to the control computer. They utilized biphasic 300 μs with 1-200 μA stimulation. The firing rate of the motor neurons was measured to control a cursor which was driven to a target on the computer screen. The threshold for the stimulation amplitude was defined as the level at which patient could feel a sensation. The upper limit of stimulation was set

as the current amplitude at which the sensation modality changed or the sensation became uncomfortable. The stimulations were delivered in 500-ms-duration pulse trains with different amplitudes and frequencies. The patients estimated sensation magnitude with open-ended numbering. After delivering 30-60 s of stimulation, the stimulation started to evoke stable sensation of pressure/touch, joint movement or joint position. By increasing the amplitude, the sensation of pressure/touch spread from distal to proximal regions. For the proprioception feedback, the stimulation caused the sense of flexion of distal joint. The increase in amplitude results in an increase of flexion and further increase of amplitude evoked sensation in the middle joint as well. In some cases, sensation of proximal joint flexion occurred.

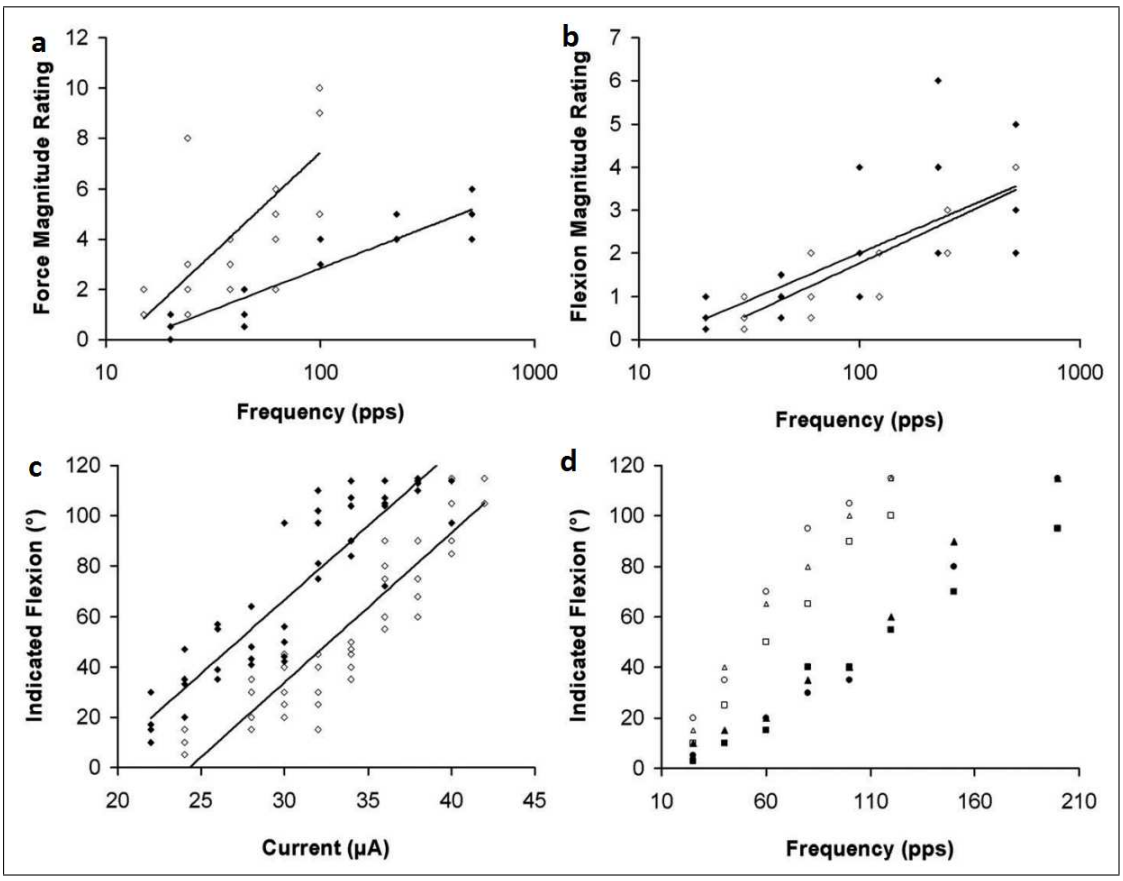

Figure 2.20 Sensation magnitude vs stimulation parameters (open symbols from the first day, the filled symbols from the seventh day (a, b, c); open symbols for 38 μA, filled symbols for 32 μA (d)) [5].

In Dhillon et al.'s study, the change in stimulation frequency changed the perceived amplitude in the defined range by not affecting the modality and the perceptive field. The rating of pressure/touch magnitude and the rating of flexion magnitude

were logarithmically correlated with the stimulation frequency (Figure 2.20a, Figure 2.20b). The Figure 2.20c and Figure 2.20d show that the perceived flexion matched to contralateral finger movement had linear correlation with stimulation amplitude and frequency. The Figure 2.20d shows the relation between the stimulation frequency and perceived flexion represented by contralateral finger. The open symbols were obtained at 38 muA and filled symbols obtained at 32 μA. Therefore, the lower stimulation amplitude required higher frequency of pulses in order to generate similar sensation. In short, the stimulation amplitude and the frequency were used to modulate the sensation intensity and perceptive field.

The sensory feedback from a robotic prosthesis enables the patients to control the device with better performance. Furthermore, stimulation of the nerve trunk may reduce the phantom limb pain. Dhillon et al. [3] extended their previous study by replacing the virtual application with a prosthetic arm. The robot had force sensor on the thumb and angle sensor on the elbow. They implanted LIFE electrodes to 6 patients who were blindfolded. Three of them were for the tactile sensation experiments and three of them for the proprioception tests. They used 300 μs biphasic controlled current stimulation and determined the amplitude for stable sensation. The modulation of the frequency provided the intensity of pressure or the elbow position.

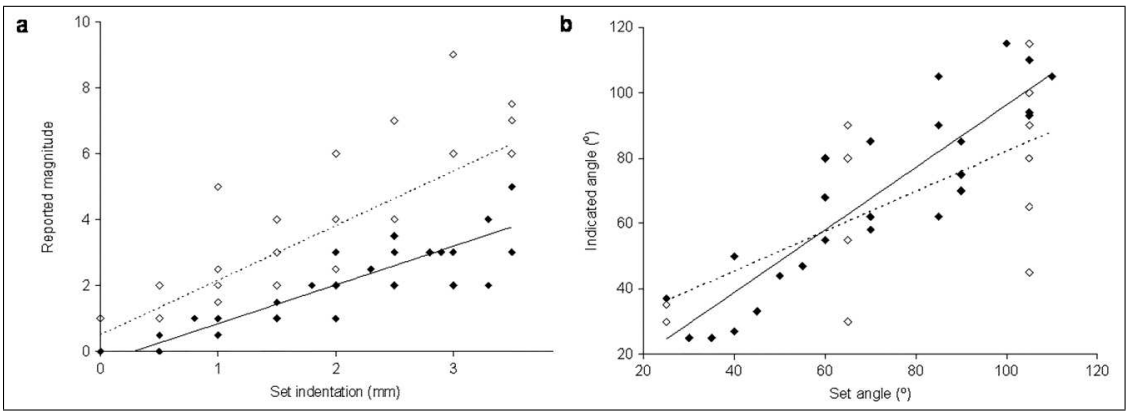

Figure 2.21 Sensory feedback and patient responses. (a) psychophysical sensation magnitude vs indentation applied on the thumb sensor. (b) Matching response with contralateral elbow movement vs set artifical limb position. (open symbols for day 1 and filled symbols for day 7) [3].

The signals form the artificial arm sensors were logarithmically converted to the stimulation frequency. The patient reported the tactile sensation amplitude with open scale estimation. There was a significant correlation between the subject estimates and

the applied force on the pressure sensor (Figure 2.21a). The estimates of artificial arm elbow position were matched by positioning the contralateral intact elbow and there was significant correlation between them (Figure 2.21b).

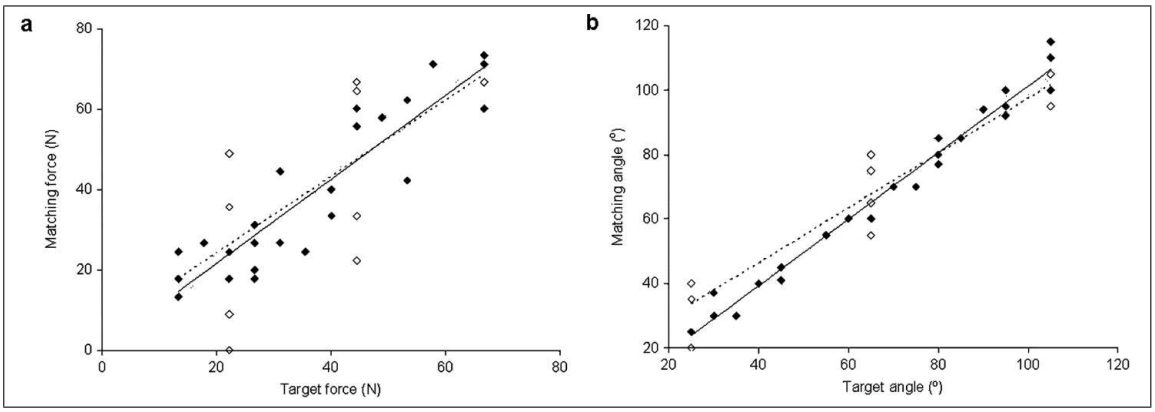

Figure 2.22 Motor output of the artificial arm. (a) The force applied by the robotic hand vs target force. (b) Postion of the robotic arm elbow vs targeted postion. (open symbols for day 1 and filled symbols for day 5) [3].

The patients were trained to control the force applied by the artificial arm and position. After training, the blindfolded patients were able to exert the targeted force by artificial hand (Figure 2.22a). There was also correlation between the target and controlled elbow positon (Figure 2.22b).

Another study by Tan et al. [2] showed that the sensory feedback from prosthesis provides better manipulation of the device. They had two subjects implanted with cuff electrodes and FINEs. One subject had 8 channels on medial nerve, 8 channels on ulnar nerve and 4 channels on radial nerve. 19 of 20 channels provided sensation at 15 unique locations (Figure 2.23). The other subject had 8 channels on the medial and 8 channels on ulnar nerve. 14 channels provided 9 unique locations.

Biphasic constant current with fixed stimulus duration and amplitude were used. With standard stimulation parameter, the patient sensed paresthesia. The perceptive area and the sensation magnitude increased with increasing amplitude and duration of stimulation (Figure 2.24). In the study, they employed pulse-width modulated stimulation with which the subjects reported more natural sensation. They used a 1 Hz sinusoidal wave to modulate the widths of 100 Hz pulses (Figure 2.25a). With the increased pulse width, the sensation became more intense. Further increase caused constant vibration, itch or tingling. When the minimum pulse width was increased the

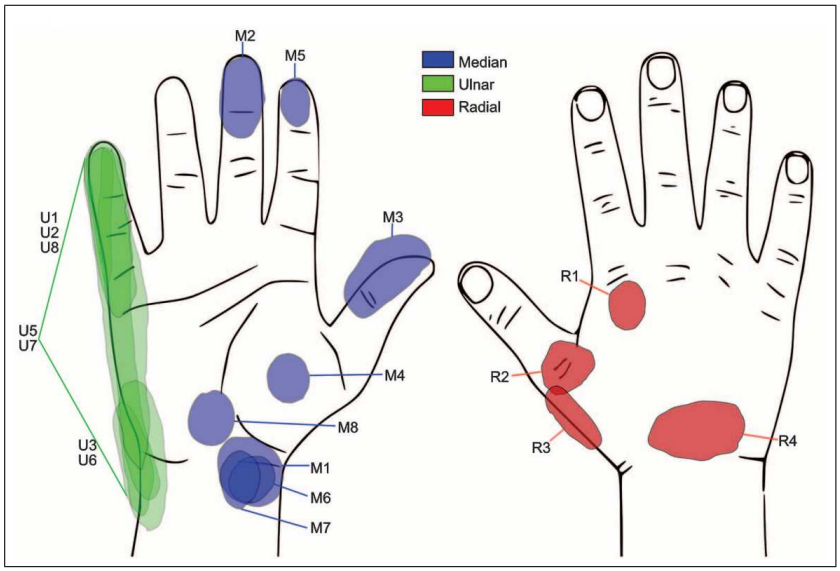

Figure 2.23 Perceptive fields of subject one [2].

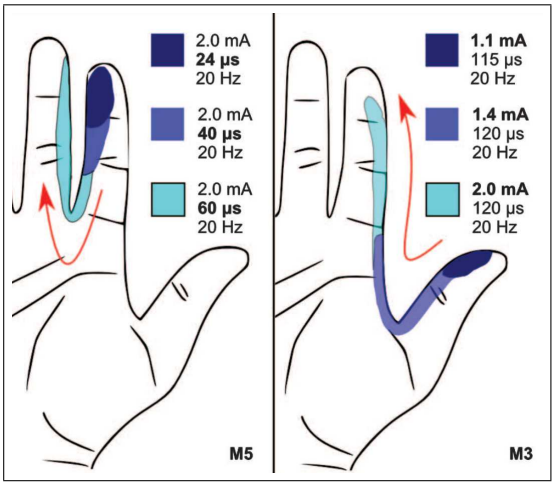

Figure 2.24 Perceptive area expands with increasing stimulation duration(left) and amplitude(right) [2].

sensation transitioned to constant pressure (Figure 2.25b).

With 1 Hz pulse-width modulation, 1 Hz vibration was sensed, and increasing the frequency caused increase in sensation frequency. In addition increase in the pulse frequency caused increase in the intensity of the sensation.

To estimate the contribution of the sensory feedback, they used a task of plucking cherries. The sensors on the fingers of the robotic hand converted tactile signals into electrical stimulation. If the subject exerted too much grip force, the cherries were crushed. With the sensory feedback, the patient successfully did the task with 100% accuracy. However, when the feedback was not used, the success rate was 77%. In

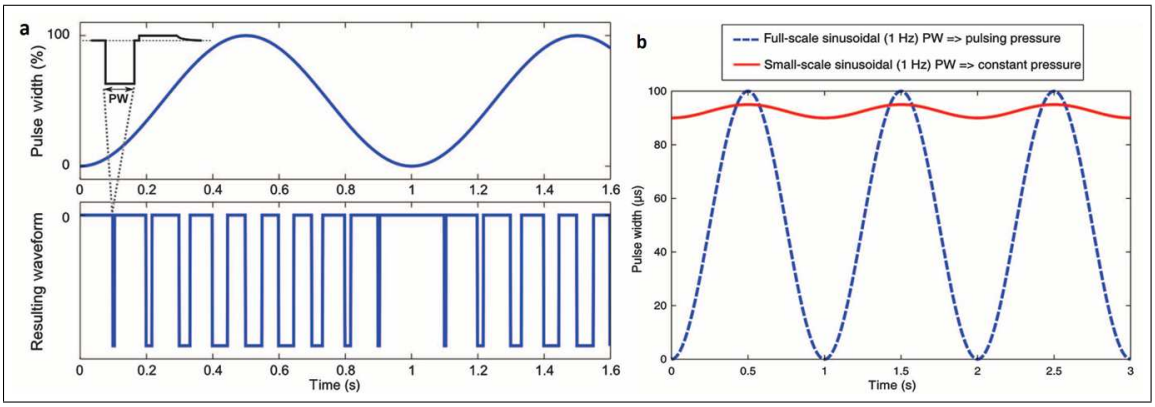

Figure 2.25 Pulse-width modulated stimulation example (a), offset pulse width modulation (b) [2].

addition, the patient had been experiencing phantom limb pain, but the episodes were diminished and they disappeared after using stimulation for a while.

In a study of Raspopovic et al. [4], a patient with amputation above the elbow could also make estimates about the properties of an object which was held with a bionic hand without auditory and visual feedback. A version of LIFE electrodes, called transversal intrafascicular multichannel electrodes, were placed in median and ulnar nerves and were used to stimulate the nerve. EMG signals are utilized to control the bionic hand movements. The stimulation via electrodes in ulnar nerve caused gradual touch sensation in little finger and the medial nerve stimulation caused artificial sensation in index and thumb. The stimulation threshold was defined as the minimum stimulus charge which elicited a sensation. The upper limit was just below the amplitude where pain was reported by the subject. The stimulation was biphasic cathodic rectangular pulses delivered at 50 Hz. The subject was able to learn control of exerted force by the artificial hand (Figure 2.26). In the staircase task the subject increased the force and reduced. He was also able to exert three discrete force amplitudes. The red arrow in little finger graph shows the overshoot where the subject was asked to exert low amplitude. His performance increased over the days of training (Figure 2.27).

The subject was able to discriminate the three levels of object stiffness. He classified the objects as hard, medium, and soft. The stiffness was coded by stimulation amplitudes of 0.67, 0.19, and 0.08 μA/s for hard, medium and soft, respectively (Figure 2.28a). The subject was also able to discriminate shapes by exploiting the differences between sensory feedbacks (Figure 2.28b). The cylindrical shape caused

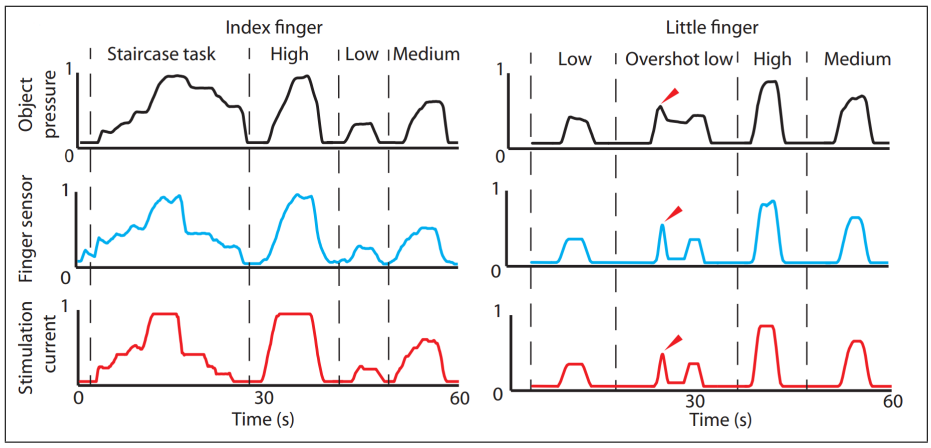

Figure 2.26 Control of exerted force by robotic hand (object pressure normalized by 1.5 kPa, hand sensor readings normalized by 60 N, stimulation amplitudes normilazed by 240 and 160 μA for index and little finger,respectivly) [4].

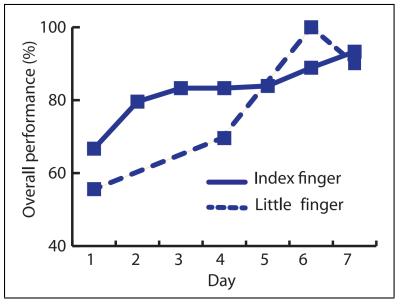

Figure 2.27 Increase in the force control performance by training [4].

pressure on both sensors while small object caused on only one. The spherical shape was recognized by the contact delay between the two sensors.

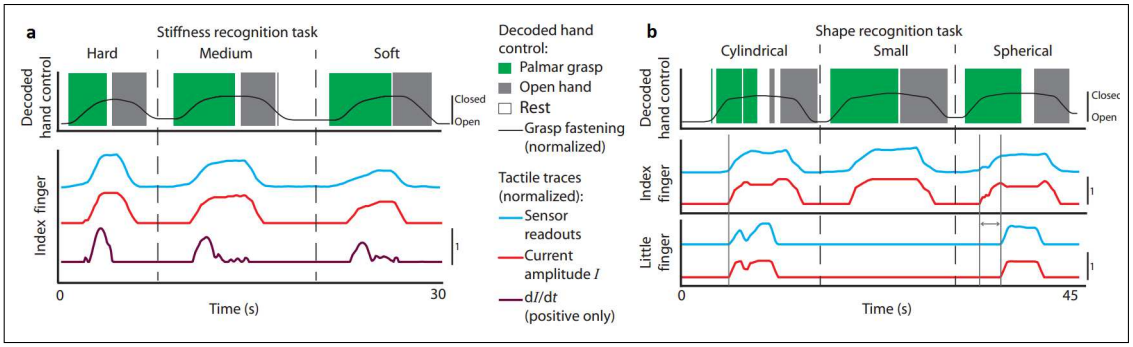

Figure 2.28 Stiffness recognition (a), shape recognition (b) [4].

3. METHODOLOGY

3.1 Animals

The experiments were conducted on 13 common water frogs (*Rana ridibunda*). The frogs were double pithed before the sciatic nerve was dissected. Both of the sciatic nerves of each animal were used in the experiments. Experiments were approved by the Institutional Ethics Committee for Animal Experiments and Care of Boğaziçi University.

3.2 Equipment

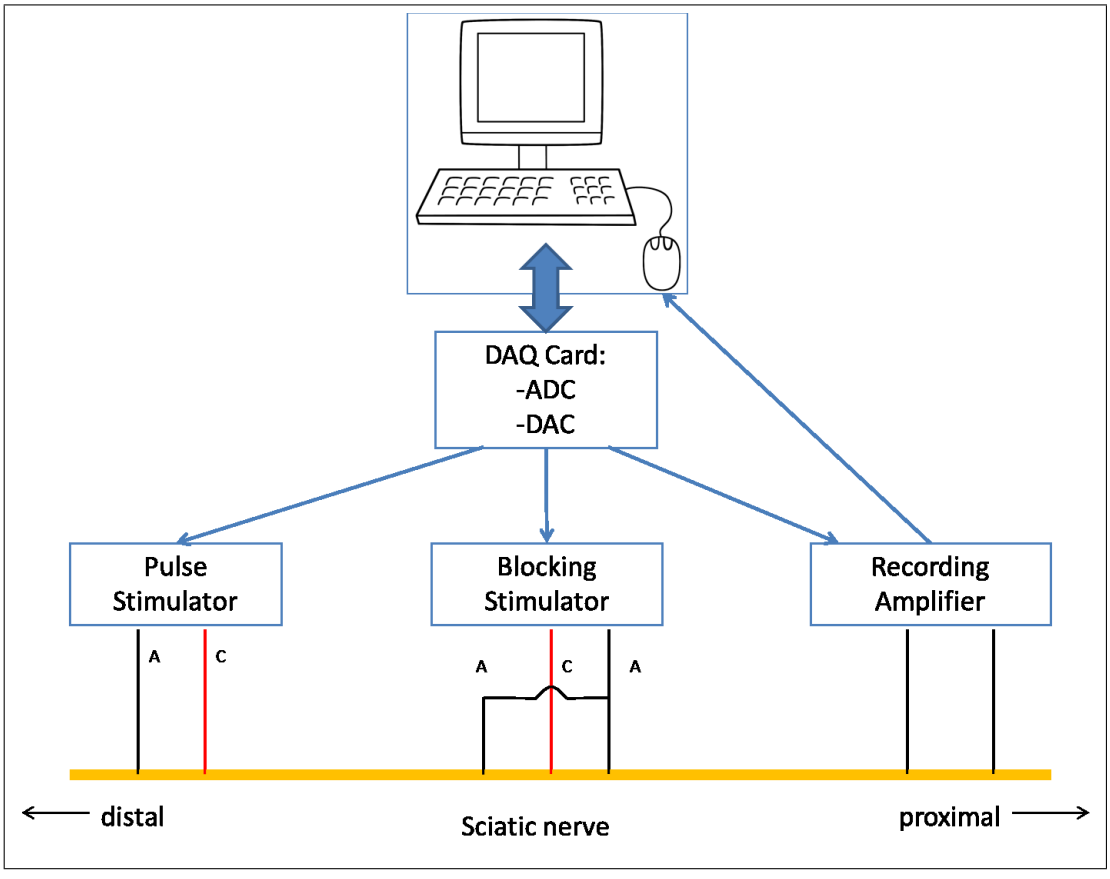

Figure 3.1 Block Diagram of the Experimental Setup.

The diagram of the setup is shown in Figure 3.1. The equipment for the experiments was controlled via a computer. The control software was developed on MATLAB (The MathWorks, R2008a). The computer had a data input/output card (DAQ) (National Instruments). Three analog output ports of DAQ were used to drive the pulse stimulator, the blocking stimulator and to trigger the recording amplifier which were isolated and battery supplied.

The pulse stimulator (A-M Systems Digital Stimulus Isolator-2003) was used to evoke compound action potential at the distal end of the nerve. The output of the stimulator was constant current whose amplitude was set manually via the knobs on the device and the duration was controlled by an analog out from the DAQ.

The blocking stimulator was a voltage controlled current source designed by Dr.Güçlü [73].The blocking stimulator follows the voltage waveform input. The blocking stimulator follows the voltage waveform input. The conversion ratio was programmed by a resistor, and was 100μA/1V.

An evoked potential amplifier (BrainQuick Matrix Acquisition, Micromed S.p.A.) was use in the differential mode to record the CAP. The amplifier had low pass filter (LPF) with cut off frequency of 4 kHz in order to reduce the high frequency noise. The high pass filter (HPF) was set to 4 Hz in order to reduce low frequency components. The CAP traces were saved by the device's software (Systemplus Evolution, Micromed S.p.A.) and then converted to .mat files online during the experiments.

3.3 Electrode Design

Based on the setup given in the Figure 3.1, a custom electrode chamber was used. The main body was made of acrylic and the electrodes were stainless steel (Figure 3.2). Approximate distances between electrodes are given in Figure 3.3. The electrodes were designed to increase the contact surface with the nerve. Each lead was designed as a pair. The pair is like a closed 'V' shape and squeezed the nerve slightly. Two distal electrodes were for pulse stimulation. The blocking stimulation was applied through next three electrodes which were in tripolar configuration (one cathode in between two

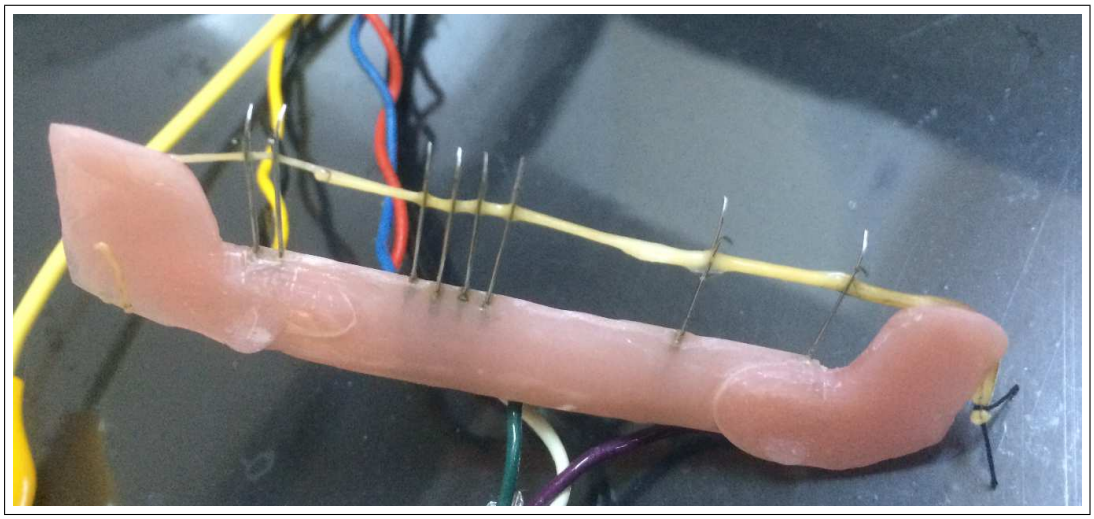

Figure 3.2 Photograph of the electrode chamber.

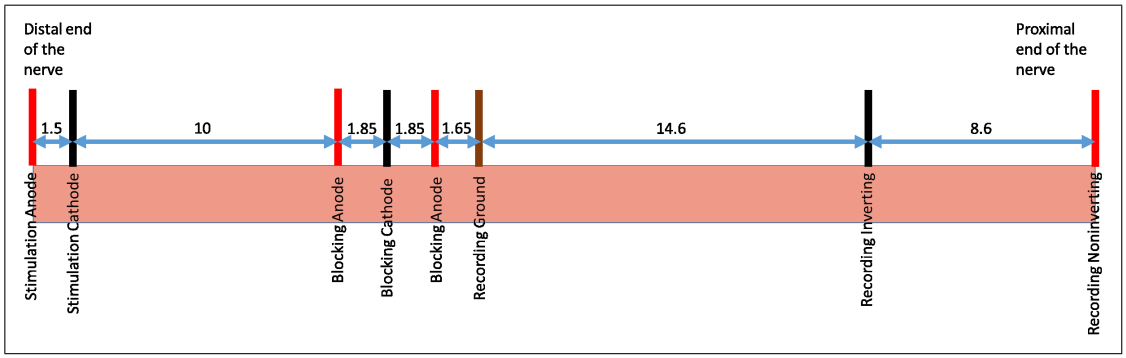

Figure 3.3 Electrode Configuration Diagram (Numbers are distance in mm).

anodes connected in parallel) in order to reduce the virtual cathode effect which might have caused undesired activation [26, 33]. The distance between the pulse stimulation electrodes and blocking stimulation electrodes were determined for the easy separation of the A component and the C component in the CAP. The ground from the amplifier was connected closely to the blocking electrodes to reduce the artifacts. Proximal two electrodes were for differential recording. The distance between them was adequate to separate the peaks in the CAP.

3.4 Surgery

The sciatic nerve was dissected and completely removed from the frog. The nerve was placed in the recording chamber in a humid environment and it was kept moist with Frog's ringer solution (112 mM NaCl, 1.9 mM KCl, 1.1 mM $CaCl_2$, 1.1 mM glucose, 2.4 mM $NaHCO_3$, and 1.0 mM NaH_2PO_4 adjusted to pH 7.2) [73].In order to maximize length, it was dissected close to the vertebra and at the end of the tibial nerve close to the ankle. The nerve had smaller diameter at the end due to the branching and the branches were cut away. Because of the larger contact area at the proximal end, the recording electrodes were positioned at that side.

3.5 Pulse Stimulation and Excitation Characteristics

The pulse stimulation was used to evoke CAPs which were used for obtaining the excitation characteristic of the nerve. The pulse stimulation was monophasic pulse with amplitude set by knobs manually and the duration was controlled by an analog output of DAQ.

An example of evoked CAP is given in Figure 3.4 - 3.5. The components due to the A fibers and the C fibers are shown in the figures. The records were post-processed with low pass filter to increase the signal to noise ratio. The cutoff frequencies were 6.5 kHz and 500 Hz for the A component and the C component, respectively.

The pulse stimulation was also used to derive strength-duration (S-D) curves. The threshold for the A component and C component were measured at different durations, respectively (Table 3.1).

Table 3.1
Stimulation Durations (μs) for the A and the C components.

A Fibers	3000	1500	1000	300	100	30	10	
C Fibers	4000	2000	1000	500	250	125	60	30

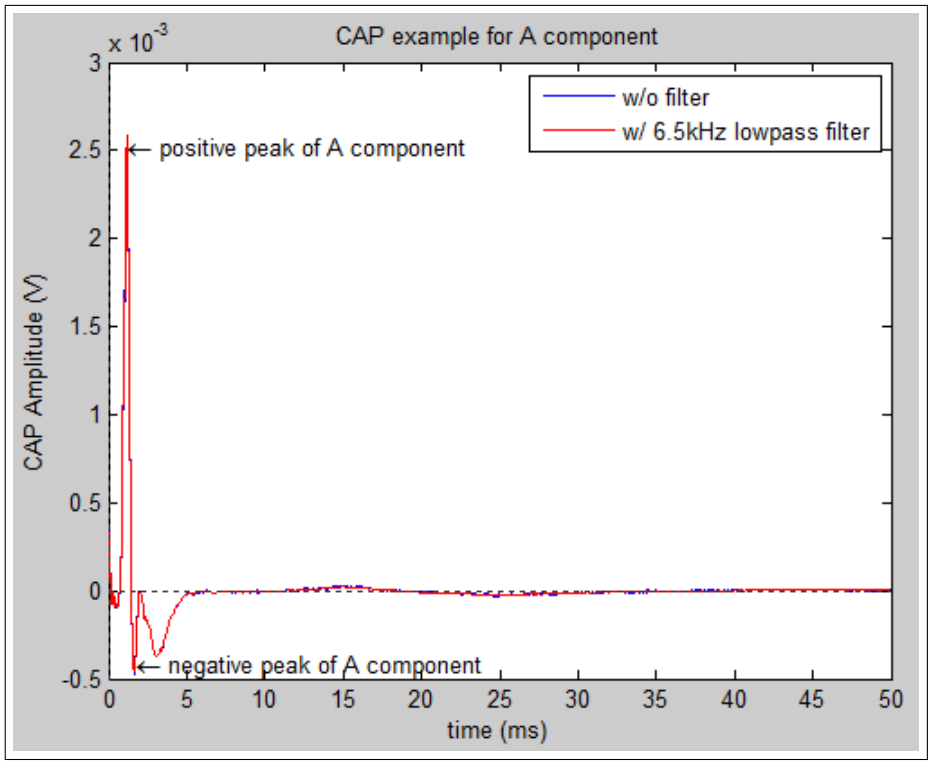

Figure 3.4 A CAP recording (blue line not filtered, red line with low pass filter).

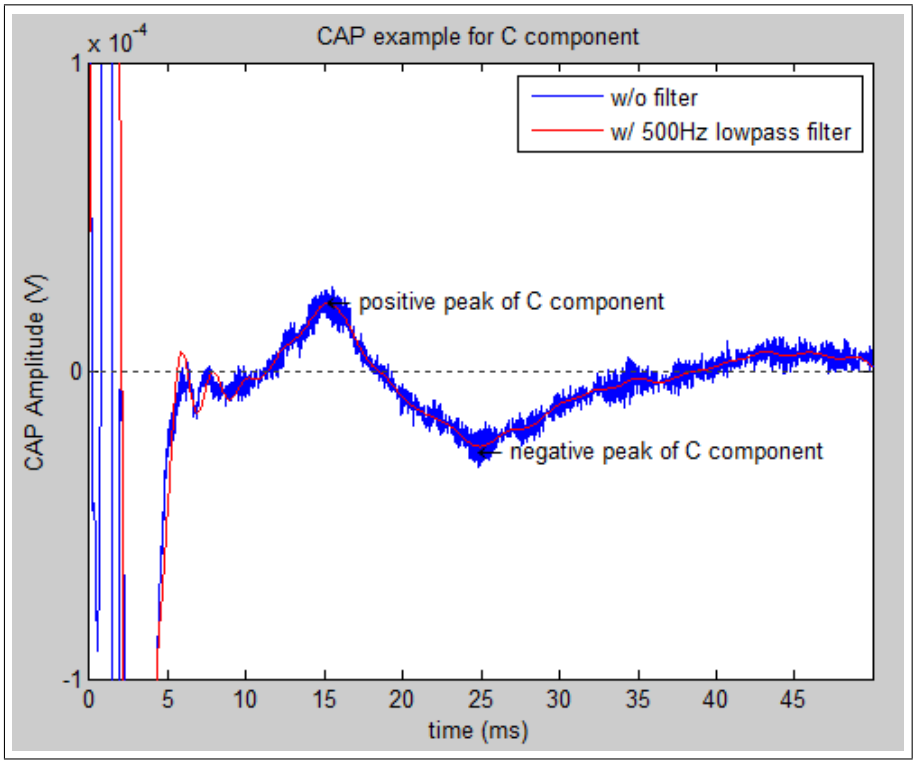

Figure 3.5 The same CAP in Fig 3.4 zoomed on the y axis (blue line not filtered, red line with low pass filter).

The pulse stimulation was repeated ten times. The threshold criterion was based on the root mean square (RMS) of the A component calculated over the time interval of 1-5 ms. If the CAP amplitude was above the 20 μV, the A component was considered to be present. On the other hand, for the C component, the RMS value of the CAP was calculated over the time interval 15-40 ms. The threshold criterion was 5 μV.

In the blocking trials, the pulse stimulation duration was set to 1000 μs which was approximately chronaxie for the C component. The amplitude was set four times of the threshold of the C component obtained when the duration was 1000 μs.

3.6 Blocking Stimulation

The blocking stimulation was a DC hyperpolarization block. It had a waveform with two parts. The first part was the plateau region which was a step function. The preliminary studies showed the C component reached the blocking side around 6 ms so a delay of 4 ms was chosen for the blocking stimulation. Therefore, the plateau region was 4-ms delayed step function with amplitude calculated as multiples of the threshold of the C component ($\frac{1}{6}$, $\frac{1}{4}$, $\frac{1}{2}$, 1 and 2 times the threshold amplitude). The lower three were pooled together for the evaluation of the blocking effect on the C component because of the small number of valid measurements. The valid trials were defined as those in which the blocking stimulation did not evoke CAP components from myelinated fibers. The plateau part lasted 4, 6 or 8 ms then, the second part of the waveform was applied. The second part was an exponential decay (time constant = 1.1×10^{-3}) to avoid anodal break excitation [28]. Their combinations account 15 different waveforms and they were applied randomly. An example is given in Figure 3.6.

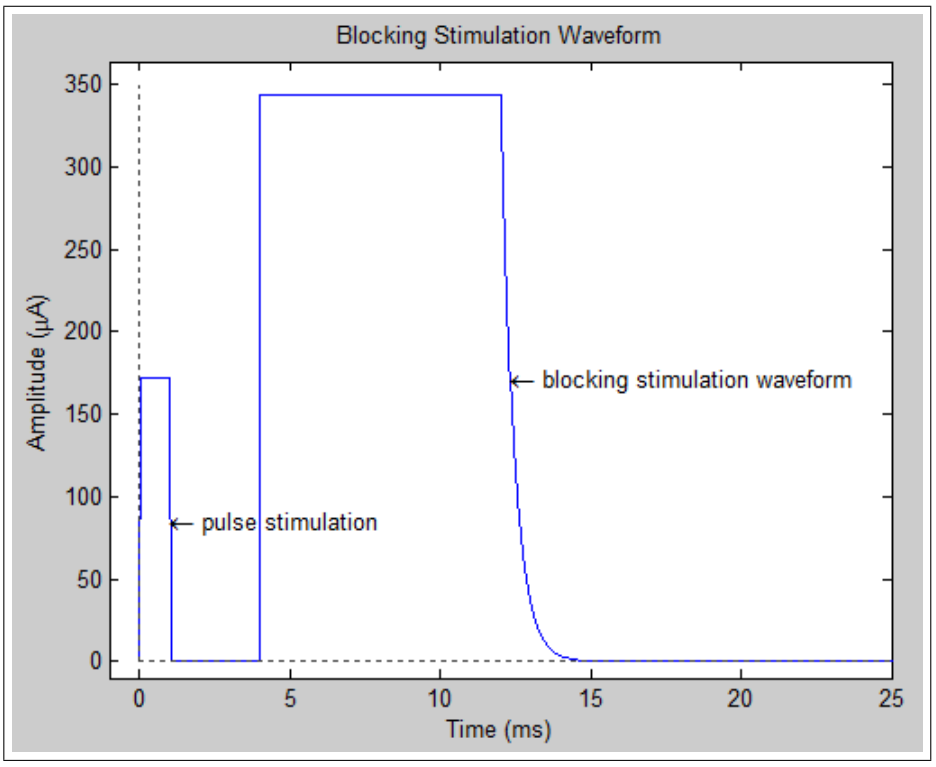

Figure 3.6 An example of pulse and blocking stimulation waveform.

3.7 Procedure

All experiments were performed in a Faraday cage. Before the start of the experiment if there was too much noise in the recording trace, the session was terminated and the other sciatic nerve of the same animal was tested. Additionally, if the threshold criterion were not met at the beginning of the experiments (nerve unresponsive or damaged) the session was terminated too. The flow chart is giving in Figure 3.7. If the initial checks were positive, the S-D cure was obtained and this ended nerve characterization protocol. Afterwards, the blocking protocol started. CAPs were measured with only pulse stimulation, only block stimulation, and finally with both pulse and blocking stimulation. Each stimulation was repeated ten times and the CAP response was averaged. This protocol was repeated for each waveform condition.

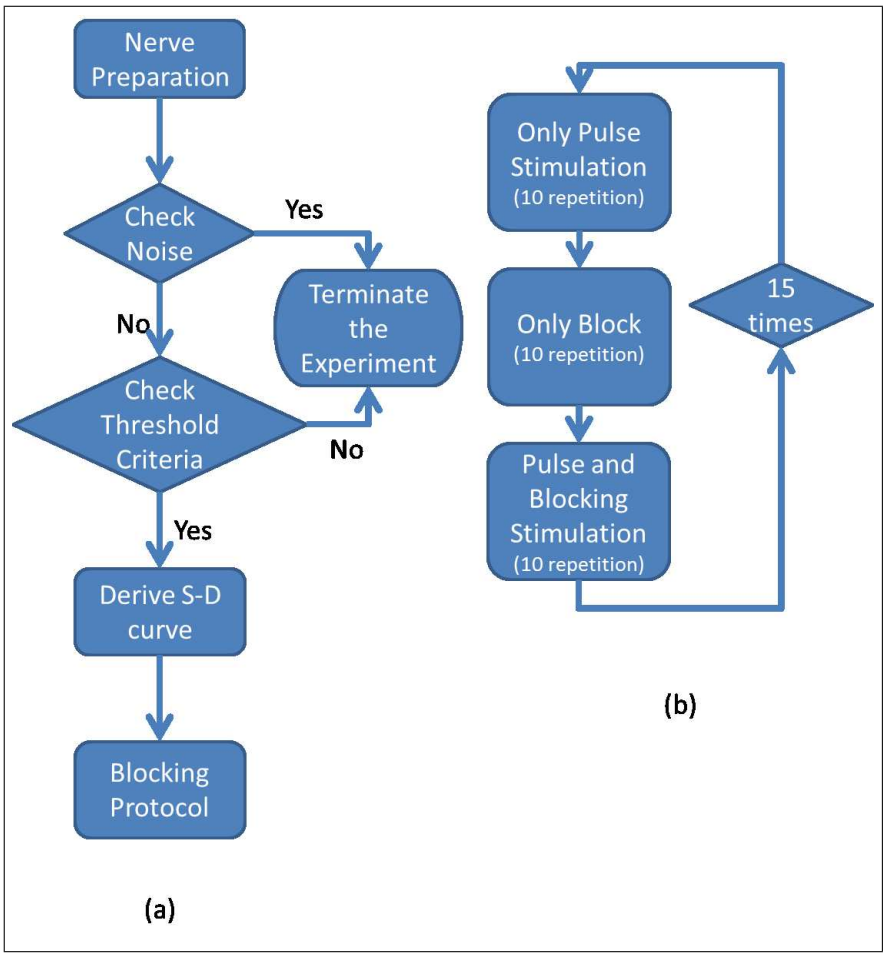

Figure 3.7 The flow chart of the procedure. a) Nerve characterization protocol. b) Blocking protocol.

3.8 Analyses

Out of 26 sciatic nerves from the frogs, 12 nerves were not used because of damage/high noise level or unresponsiveness. The remaining nerves were used for obtaining S-D curves and conduction velocities. The conduction speeds were calculated form the delays of the positive peaks. Lapicque and Weiss equations were fitted to the data points of the S-D curves. Rheobase and chronaxie were calculated from the equations.

302 trials were completed on 14 functional nerves. Due to the long duration of the experiment, the function of the nerve was tested by measuring the response of the A component before and after the blocking protocol. Additionally, the blocking stimulation sometimes caused another A component. The effects of blocking stimulation parameters on this component were studied by using Pearson's correlation analysis. For this purpose, peak to peak amplitudes of the A component evoked by the blocking

stimulation in each trial of a session was normalized with the maximum peak to peak A component evoked in the entire session.

67 trials were evaluated for the effect of blocking on the C component. The rest of the trials were not included in the analysis because the blocking stimulation caused another A component or due to missing data. Blocking stimulation also caused an artifact which partially overlapped with the C component. Therefore, the C component analysis was done 2 ms after the blocking stimulation ended. Three amplitude levels of blocking stimulation and durations were tested. The dependent variable was the ratio of the RMS value of the C component after the block to RMS value before the block. The ratios were input to the aligned rank transform (ARTool) [74]. The transformed values were analyzed by ANOVA.

4. RESULTS

4.1 Conduction Speed

The positive peak of the components was used to calculate the conduction speed with $speed = distance/time$ formula. The gap of 29.95 mm between the negative electrode of the pulse stimulator and the inverting electrode of the recording amplifier was the distance of propagation. The delay time between stimulation and the arrival of the positive peak of the A component or C component were used in the formula. The conduction speeds of the A component and C component are given in Table 4.1.

Table 4.1
Conduction speeds of A and C components in CAP recordings.

Subject	A Fibers (m/s)	C Fibers (m/s)
F141202R	42.67	1.67
F141209L	42.67	1.43
F141209R	42.67	1.43
F141216L	44.61	1.64
F141218L	39.26	1.38
F150306L	42.67	1.78
F150313R	28.04	1.78
F150316L	51.65	1.64
F150316R	42.67	1.64
F150318R	44.61	1.97
F150324R	22.82	1.07
F150325R	29.74	2.07
F150326L	49.07	2.10
F150326R	51.65	1.79
Mean	41.06	1.67
Std	8	0.26

An independent-sample t-test was conducted to compare the conduction speeds of both components. There was a significant difference between the conduction speed of A components and conduction speed of C component ($t(26) = 17.13$, $p < 0.001$). As expected the mean conduction speed of the A component (41.06 m/s) was much higher than the speed of the C component (1.67 m/s).

4.2 Excitation Characteristics

Distal pulse stimulation was used to evoke action potentials in sciatic nerve. The S-D curves of A components and C components for 14 subjects are given in Figure 3.4 and Figure 4.2, respectively. The means and standard deviations of the data across subjects are given in Figure 4.3 and Figure 4.4. Additionally, the means and the standard deviations for each pulse duration are listed in Table 4.2.

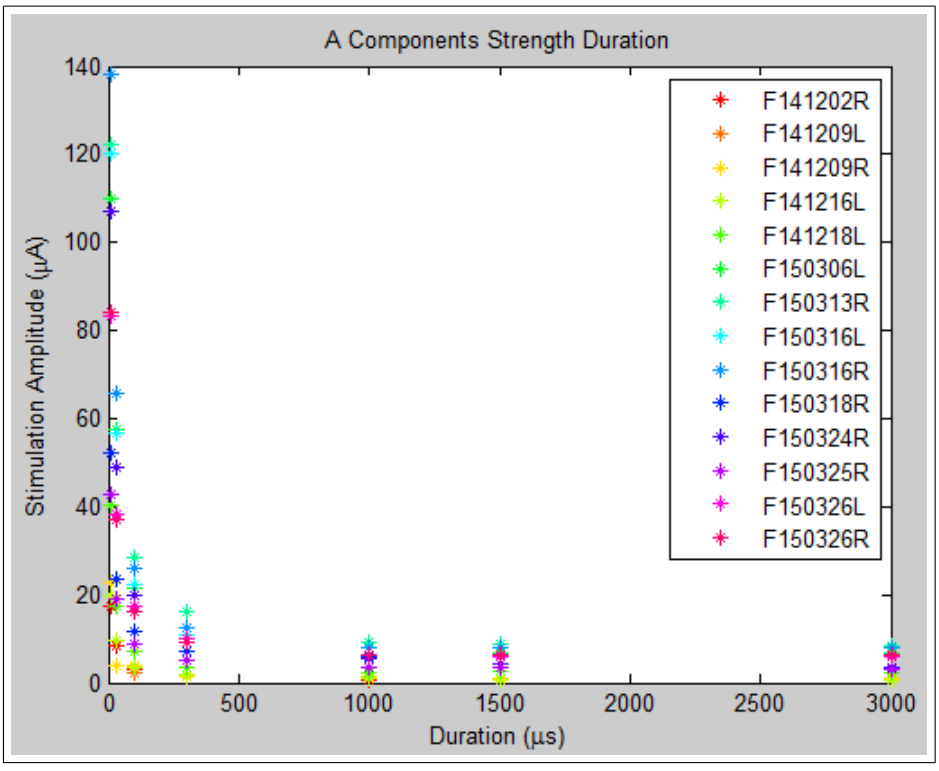

Figure 4.1 Excitation characteristics of the A components from each subject.

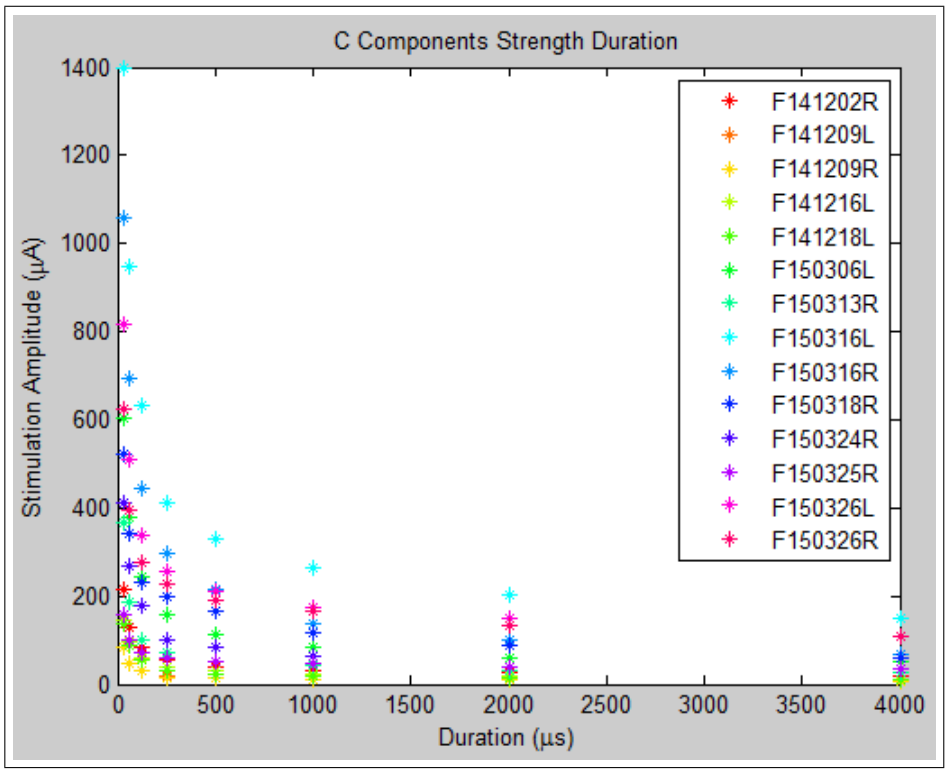

Figure 4.2 Excitation characteristics of the C components from each subject.

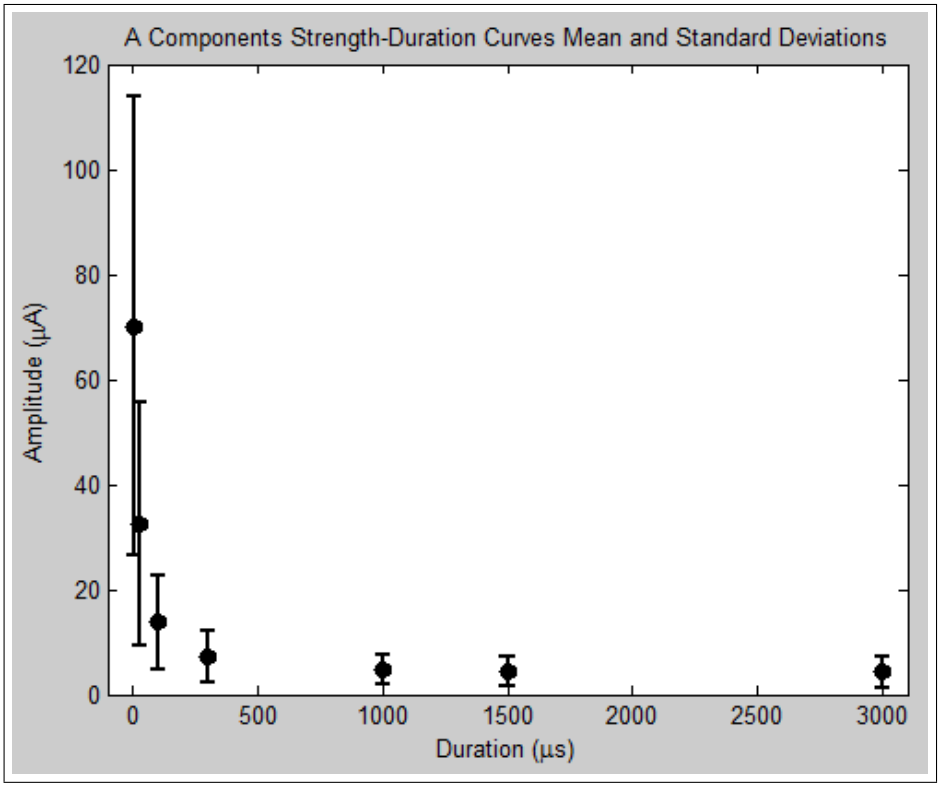

Figure 4.3 Excitation characteristics of the A component across every subjects (error bar: standard deviation).

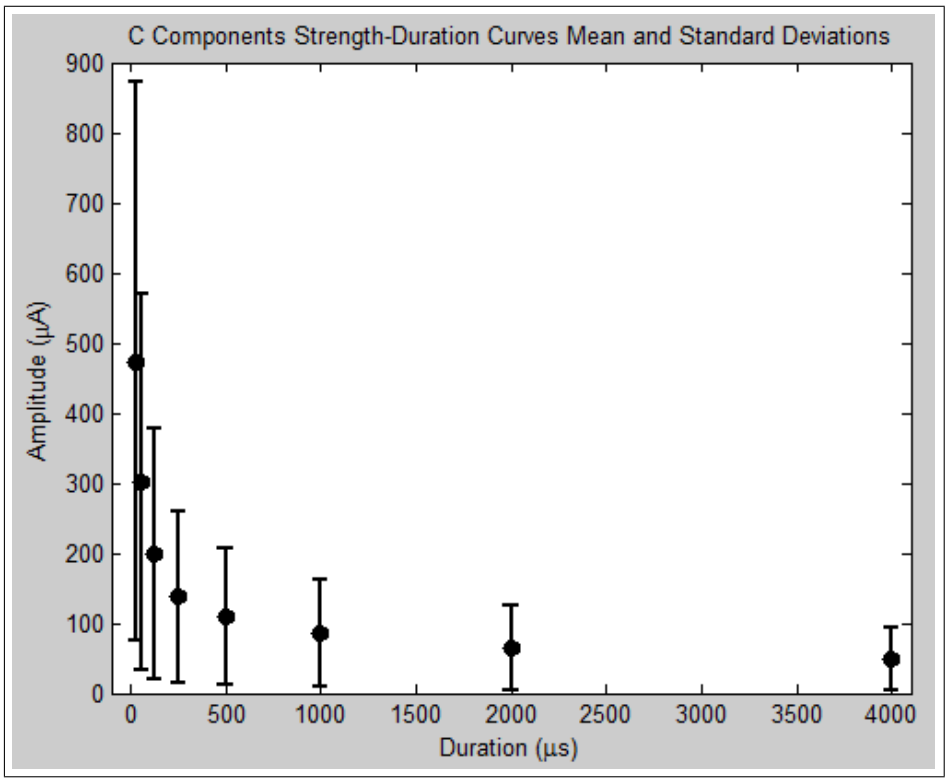

Figure 4.4 Excitation characteristics of the C component across every subjects (error bar: standard deviation).

Table 4.2
Mean and standard deviation of excitation characteristic for A and C fibers.

A Fibers			C Fibers		
Duration (μs)	Mean (μA)	Std (μA)	Duration (μs)	Mean (μA)	Std (μA)
3000	4.27	2.88	4000	48.44	45.81
1500	4.41	2.83	2000	64.09	61.95
1000	4.65	2.87	1000	84.84	76.41
300	7.29	4.86	500	109.44	97.05
100	13.71	9.08	250	137.77	122.06
30	32.50	23.15	125	198.09	178.54
10	70.16	43.71	60	301.69	268.00
			30	473.47	399.09

In order to fit S-D curves shown above, Lapicque and Weiss equations are used [75]. Lapicque equation is defined as:

$$I = \frac{I_{rh}}{1 - e^{-t/\tau_{sd}}} \tag{4.1}$$

Here I stands for pulse stimulation amplitude, I_{rh} is the rheobase current and τ_{sd} is the chronaxie duration, and t stands for the pulse stimulation duration. Another model used is the Weiss equation:

$$Q = I_{rh} \times (t + \tau_{sd}) \tag{4.2}$$

When both sides of the Equation 4.2 are divided by t:

$$I = I_{rh} + \frac{I_{rh} \times \tau_{sd}}{t} \tag{4.3}$$

As can be deduced from the formulae, Equation 4.1 has an exponential decay based on duration, and Equation 4.3 is similar to a shifted hyperbole. Matlab Curve Fitting Toolbox was used to fit the equation by defining the equations and data were fed. The results of curve fitting are given in Table 4.3 and Table 4.4. As can be seen from the R^2 values, the fits were very accurate. Additionally, both equations were fitted based on data average across subjects. The row before the second from the last shows the rheobase and chronaxie values obtained from the fits of the averaged data. The mean and the standard deviation show columns statistics from the individual subject's fitting.

Independent-sample t-tests were conducted to compare rheobase currents and chronaxie durations for A component and C component obtained from Lapicque equation fitting. There was a significant difference between the rheobase values ($t(26) = 3.80$; $p < 0.001$). As expected the rheobase current of C component (88 μA) was higher than the rheobase current of A component (6.06 μA). However, there was no significant difference in the chronaxie durations ($t(26) = 1.2$; $p = 0.24$). The mean chronaxie duration of the A components was 146 μs and the mean chronaxie duration for C components was 177 μs. Furthermore, the variances of Lapicque parameters were

Table 4.3
Rheobases and chronaxies according to Lapicque equation.

	Lapicque Fitting					
	A Fibers			C Fibers		
Subject	Rheobase (μA)	Chronaxie (μs)	R^2	Rheobase (μA)	Chronaxie (μs)	R^2
F141202R	1.13	158	0.98	31	198	0.98
F141209L	0.57	371	0.96	12	196	0.99
F141209R	0.82	259	0.96	12	204	0.99
F141216L	1.32	152	0.98	23	187	0.96
F141218L	3.04	130	0.99	19	215	0.97
F150306L	9.67	114	0.97	87	204	0.97
F150313R	13.55	90	0.95	36	287	1.00
F150316L	9.08	132	0.98	274	149	0.94
F150316R	11.06	124	0.98	155	205	0.95
F150318R	6.88	72	0.99	125	117	0.91
F150324R	7.11	151	0.98	63	196	0.96
F150325R	4.34	96	0.98	47	89	0.96
F150326L	8.33	98	0.98	177	129	0.97
F150326R	7.99	103	0.99	166	101	0.95
Averaged data points	6.07	114	0.98	88	155	0.96
Mean	6.06	146	0.98	88	177	0.96
Std	4.21	79	0.01	80	54	0.02

Table 4.4
Rheobases and chronaxies according to Weiss equation.

	Weiss Fitting					
	A Fibers			C Fibers		
Subject	Rheobase (μA)	Chronaxie (μs)	R^2	Rheobase (μA)	Chronaxie (μs)	R^2
F141202R	1.05	163	0.99	26	222	0.98
F141209L	0.18	1196	0.97	10	225	0.98
F141209R	0.47	456	0.97	9	239	0.98
F141216L	1.23	156	0.99	20	203	0.97
F141218L	2.66	144	1.00	16	238	0.96
F150306L	8.98	118	1.00	74	223	0.99
F150313R	12.65	91	1.00	27	268	0.99
F150316L	8.25	140	0.99	238	156	0.97
F150316R	10.01	132	1.00	135	219	0.94
F150318R	6.07	77	1.00	109	119	0.93
F150324R	6.51	159	0.98	54	211	0.98
F150325R	3.86	103	1.00	41	87	0.98
F150326L	7.44	104	1.00	151	135	0.97
F150326R	7.01	112	1.00	145	102	0.99
Averaged data points	5.46	122	0.99	75	165	0.98
Mean	5.46	225	0.99	75	196	0.97
Std	3.93	294	0.01	70	72	0.02

studied by using the F test. There was a significant difference between the variances of the rheobase values ($F(13,13) = 0.0028$; $p < 0.001$). However, the variances of the chronaxie values were not significantly different.

Similar analyses were performed on the results from fitting according to the Weiss equation. The rheobase and the chronaxie values were similar to those obtain form the Lapicque equation. Again, the rheobase currents of the A component were smaller than those of the C component ($t(26) = 3.74$; $p < 0.001$). There was no statistically significant difference between the chronaxie durations of the A and C components ($t(26) = 0.25$; $p = 0.72$). The F test for variances gave similar results. There was a significant difference in rheobase variances. However, for Weiss fitting, the chronaxie variances were also statistically different ($F(13, 13) = 16.5$; $p<0.001$).

These results confirmed that the rheobase for the A component were smaller than the C components .This means A fibers are excited with lower current amplitudes than C fibers with long duration pulses. On the other hand, the mean chronaxies were not different between the fiber classes, which show that they would require similar pulse durations for the most energy efficient stimulation.

4.3 Electrical Charge Applied During Blocking Stimulation

The pulse stimulation and the block stimulation had non zero average current values. This offset charge might have caused damage in the nerve. In order to test for any damage, the RMS amplitude of the A component was calculated before and after blocking stimulation. The ratio of the RMS after stimulation to before stimulation was plotted against the total charge applied during the blocking stimulation (Figure 4.5). The Pearson's correlation between this ratio and the total charge was found to test for any damage. There was no correlation between two variables ($N = 363$; $r = -0.02$, $p = 0.7$). If there were damage due to blocking stimulation one would expect RMS ratio decrease from one as the total charge increased.

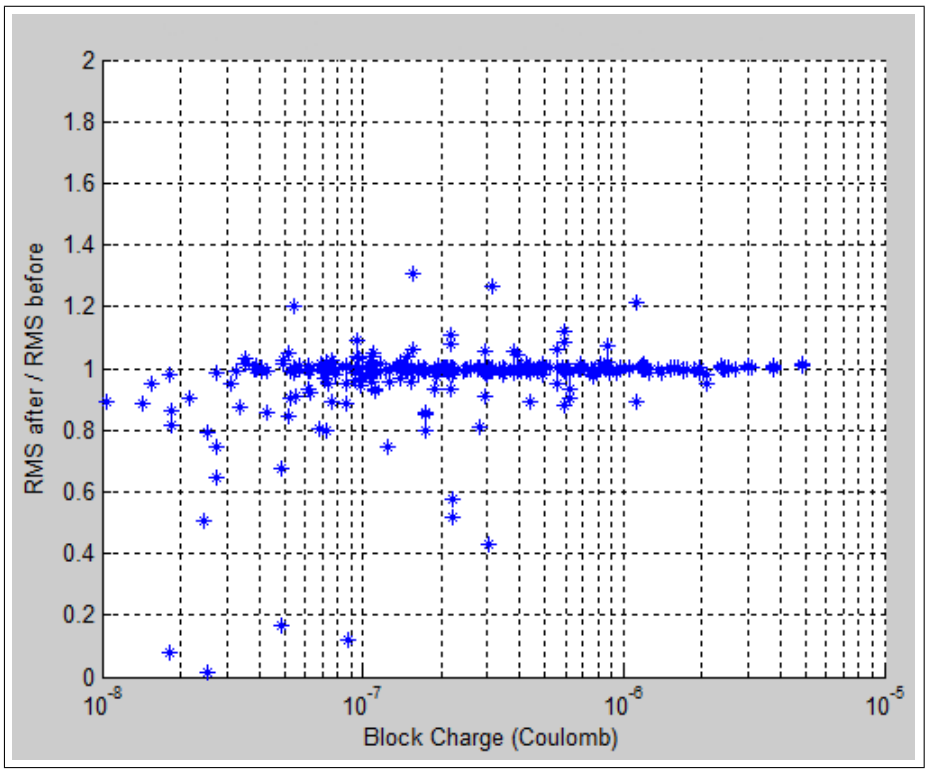

Figure 4.5 The change in the RSM value of the A component as a function of total charge applied to the sciatic nerve.

4.4 Evoked A Response Due to the Blocking Stimulation

Blocking stimulation sometimes also evoked action potential like a normal stimulation instead of blocking (see discussion for interpretation of this result). Figure 4.6 demonstrates this phenomenon. The blocking stimulation amplitudes were 323 μA ad 43 μA for the blue and green traces, respectively. The block durations (6 ms) and block delays (6 ms) were the same for both traces. The start of the block stimulation is shown by vertical dashed black line at 6 ms. Although, the blue trace was obtained by a higher block stimulation, this did not excited A fibers. The trace only shows the artifact of the block stimulation. On the other hand, there is a clear component due to the excitation of the A fibers in the green trace.

Three blocking stimulation durations and two blocking stimulation delays were tested further. The correlation between the block stimulation amplitude and the amplitude of the A component were studied. Figure 4.7 is an example of the case in which the duration is 4 ms and the delay is 4 ms. No trend can be seen in this plot. Correlations were performed for each combination of block duration and block delay

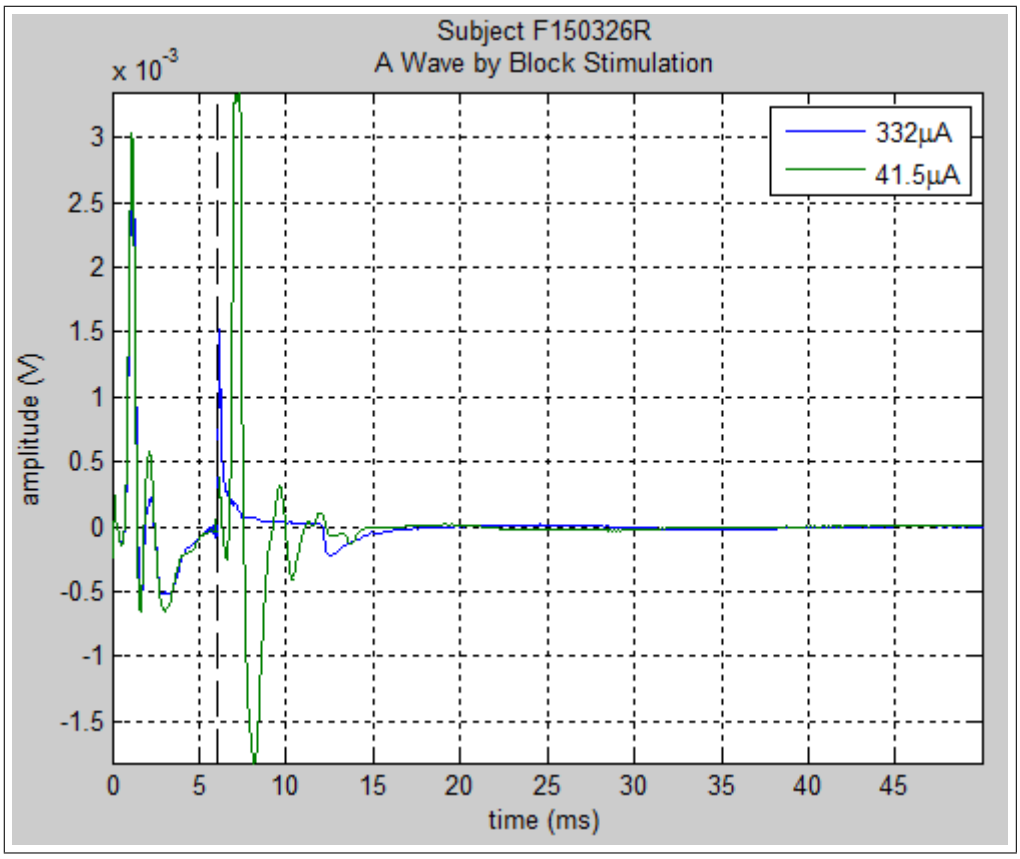

Figure 4.6 Two traces from the same subject with different block amplitudes. For both, block duration was 6 ms, block delay was 6 ms. Block amplitude : 332 μA (blue), block amplitude: 41.5 μA (green). Vertical dashed line is start of the blocking stimulation.

(Table 4.5). The independent variable were selected as either as the blocking stimulation amplitude (μA) or the blocking stimulation amplitude relative to the threshold of the excitation at 1 ms. The dependent variable was the ratio of the A component (peak to peak amplitude divided by the maximum peak to peak amplitude of the given subject). Table 4.5 shows an as the sample size which includes different blocking stimulation amplitude levels from all subject. Significant correlation was found only in some combinations of block duration and delay. The correlation was obtain with block duration of 4 ms and block delay of 6 ms. As the block stimulation amplitude increased, the A component ratio decreased (r=-0.57, p$<$0.001). Similarly as the block level (relative to the excitation threshold) increased, the A component ratio decreased (r=-0.5, p=0.001). Sometimes anodal break excitation also occurs at the offset of the blocking stimulation. Interestingly, this phenomenon did not occur if the block did not cause the activation of A fibers at the onset.

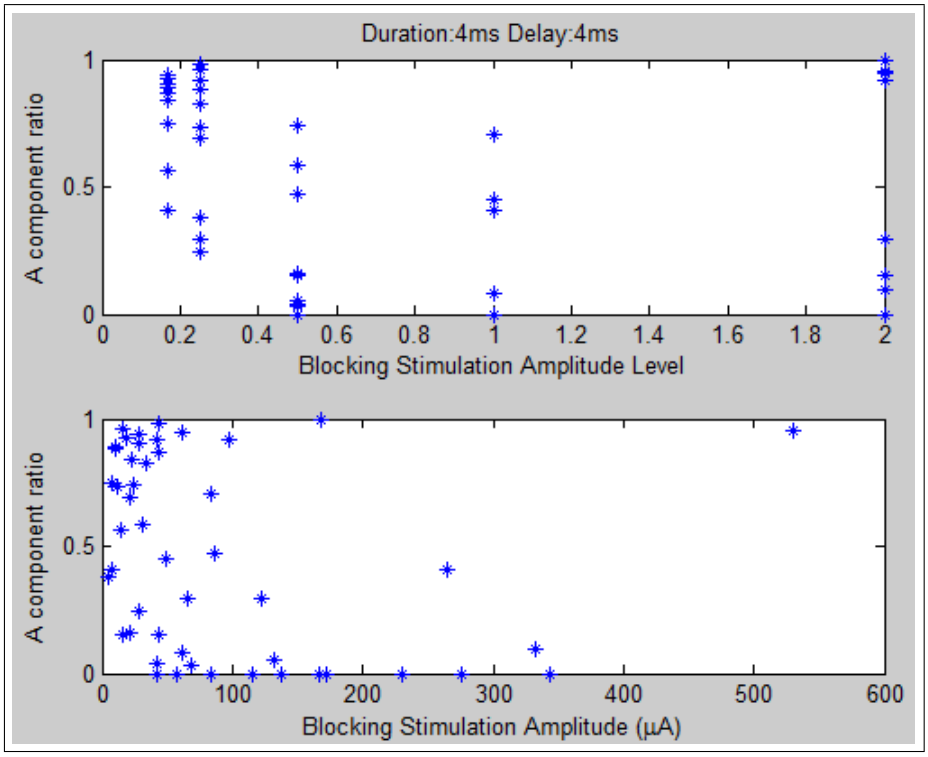

Figure 4.7 Normalized A component evoked by the blocking stimulation.

Table 4.5
Correlation table of A component evoked by the blocking stimulation.

Duration (μs)	Delay (μs)	n	r (amplitude)	p (amplitude)	r (block level)	p (block level)
4000	4000	49	-0.243	0.092	-0.291	0.043
4000	6000	44	-0.579	0.000	-0.500	0.001
6000	4000	56	-0.048	0.728	-0.132	0.333
6000	6000	47	-0.295	0.044	-0.236	0.110
8000	4000	47	-0.293	0.045	-0.351	0.015
8000	6000	49	-0.250	0.083	-0.369	0.009

4.5 Effects of Blocking Stimulation on C Fibers

Three examples of the block effect are given in Figure 4.8, 4.9, 4.10. Figure 4.8 shows the best block obtained during the experiments. The ratio of the RMS value of the C component with the block to the RMS value before the block was 0.37. In Figure 4.9, this ratio was 1.055 which shows no effect. In Figure 4.10, on the other hand, the blocking stimulation actually increased the C component to its 2.4 times to its original RMS value. In these traces the RMS value of the C component was calculated after the gray vertical line until 40 ms.

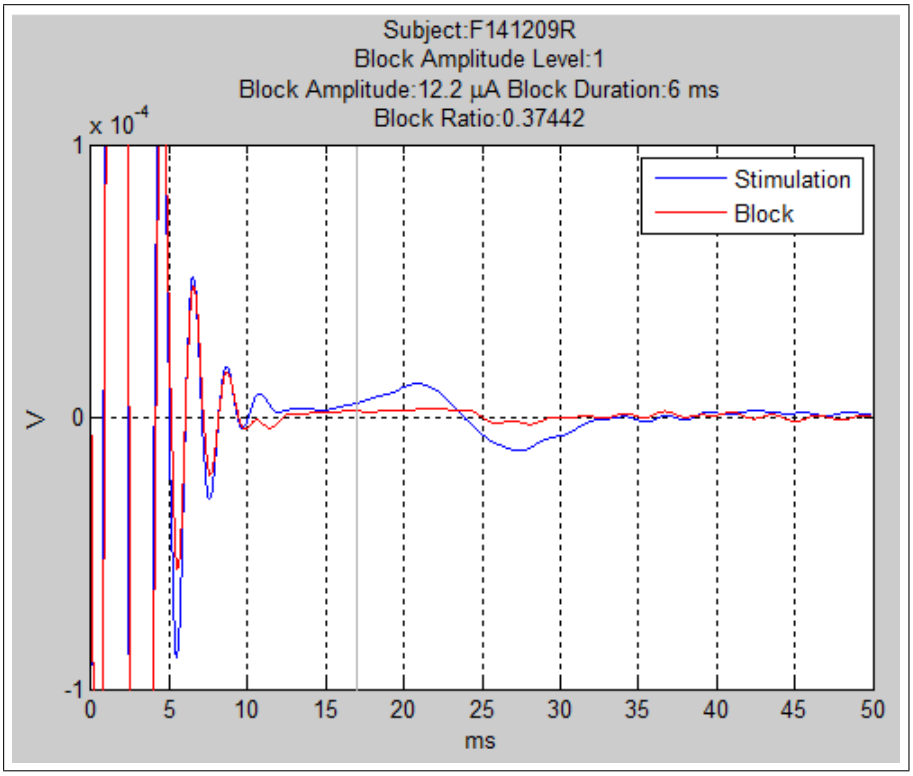

Figure 4.8 The best block obtained during the experiments (the gray vertical line is the end of the artifact).

Valid trials were defined as the ones in which the blocking stimulation did not cause excitation of the A fibers. Figure 4.11 shows the blocking effect (the ratio of the RMS value of the C component with blocking stimulation to that by pulse stimulation) as a function of blocking stimulus duration and amplitude. The data points are given by red asterisk. Black dots are the mean values. Error bars are the standard

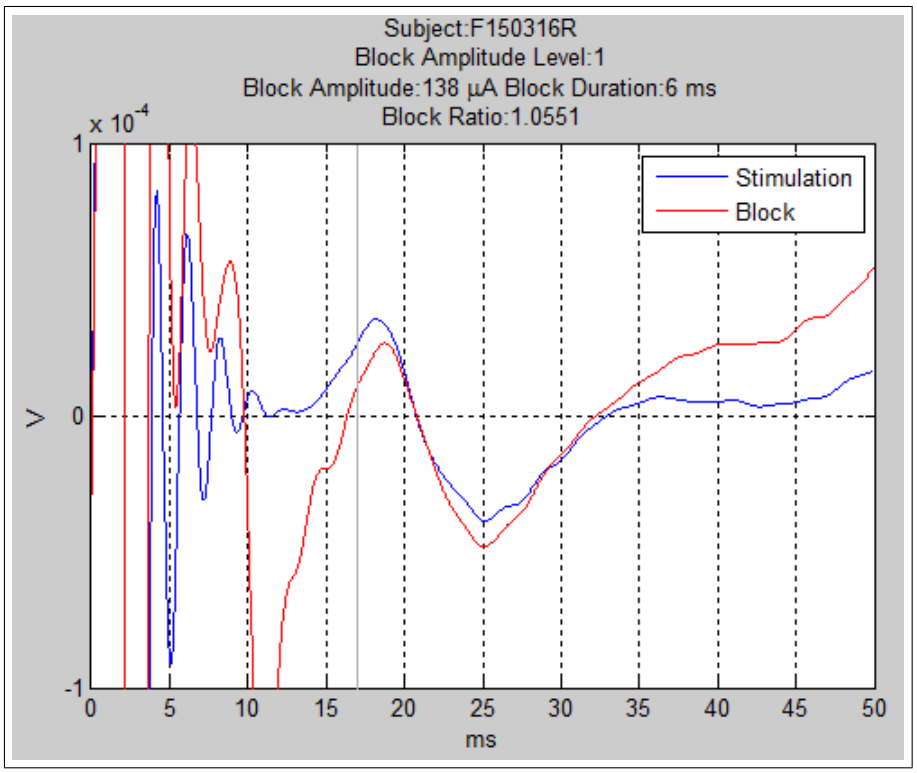

Figure 4.9 After the artifact the RMS value of the C component with the block is similar to that without (the gray vertical line is the end of the artifact).

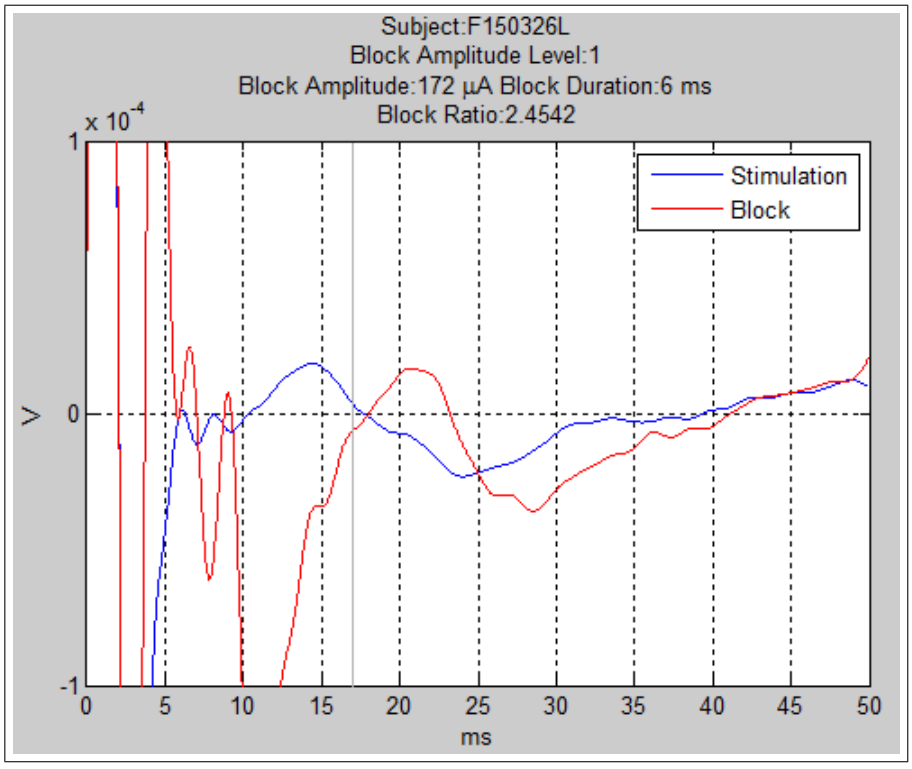

Figure 4.10 Due to the artifact, the block stimulation seems to have caused a larger C component calculated as the RMS value (the gray vertical line is the end of the artifact).

deviations. The colored surface is an interpolation according to the data points. Here, a ratio below one shows a good blocking effect. The surface suggests that for optimum blocking condensations, the amplitude of the blocking stimulus should be high but the duration should attain an intermediate value. Figure 4.12 shows some of the data from Figure 4.11. However, this time, the x axis shows amplitude relative to the excitation threshold. As Figure 4.11, higher block stimulation amplitudes seem to cause better blocks at intermediate durations.

Because of the large variance in the block ratios, I studied the distribution of the ratios among all the valid trials. Figure 4.13 shows the histogram for this distribution. There are 30 trials which result in a ratio less than one. However, 37 trials result in higher ratios. Therefore, the C component was reduced in 44% of the valid trials. The histogram also shows that the ratios smaller than 0.5 did not occur. There was a more or less uniform count distribution between 0.5 and 1. Above one, the counts decreased as block ratio increased.

The change of C fibers responses with the blocking stimulation were input to a two-way ANOVA after Aligned Rank Transform having three levels (amplitude: 0.5, 1, 2; duration: 4, 6, 8 ms). There was no significant main effect due to amplitude level ($F(2, 58) = 1.54$, $p = 0.22$). There was also no significant main effect due to blocking stimulus duration ($F(2, 58) = 0.14$, $p = 0.87$). The interaction between the factors was not significant either. In summary, the blocking stimulus amplitude level and duration did not influence the reduction in the RMS value of the C component.

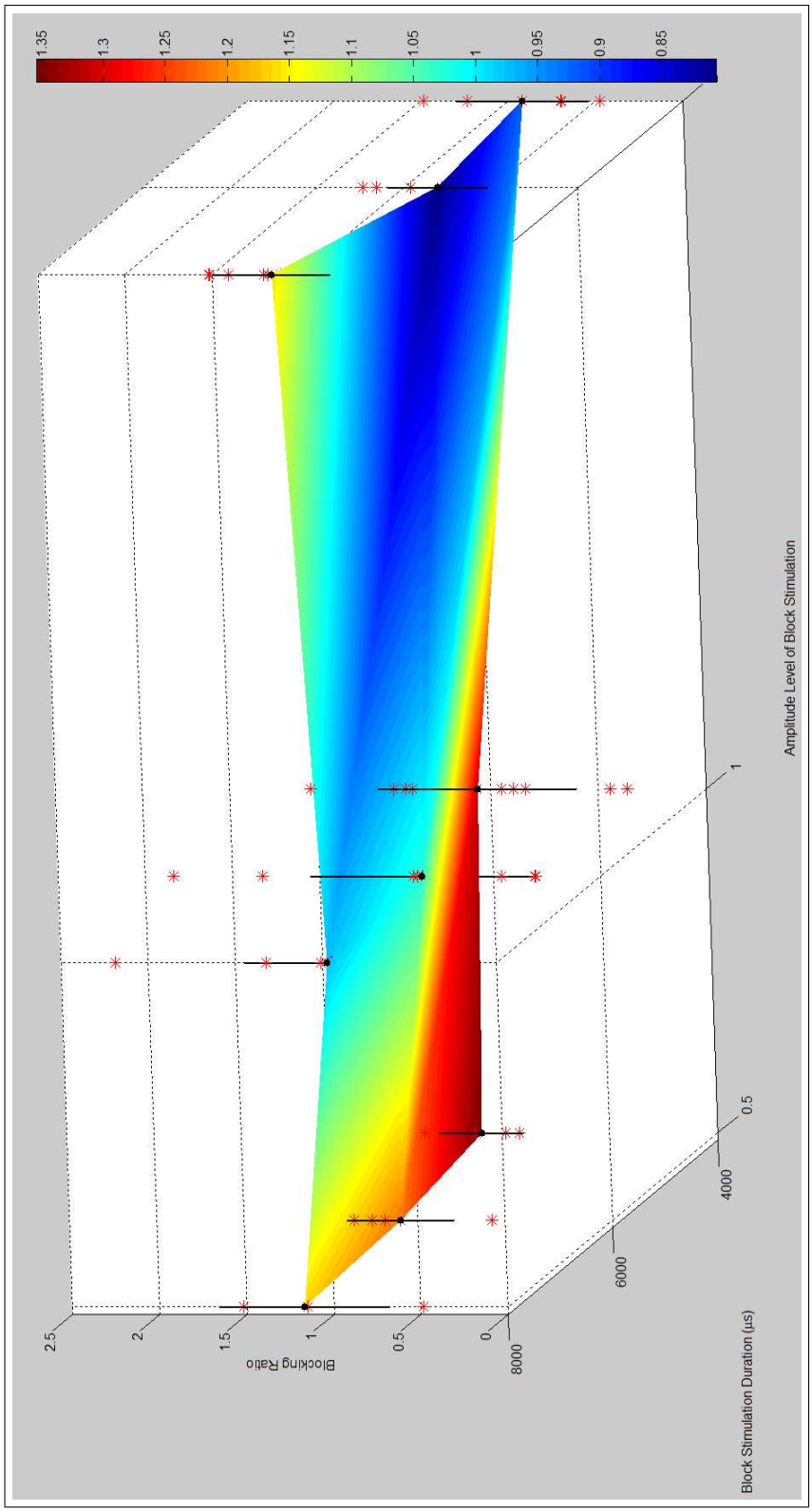

Figure 4.11 All valid blocking trials are given by red asterisks. The black dots are the means of the data points. Error bars are the standard deviations. Colored surface is an interpolation through the mean data.

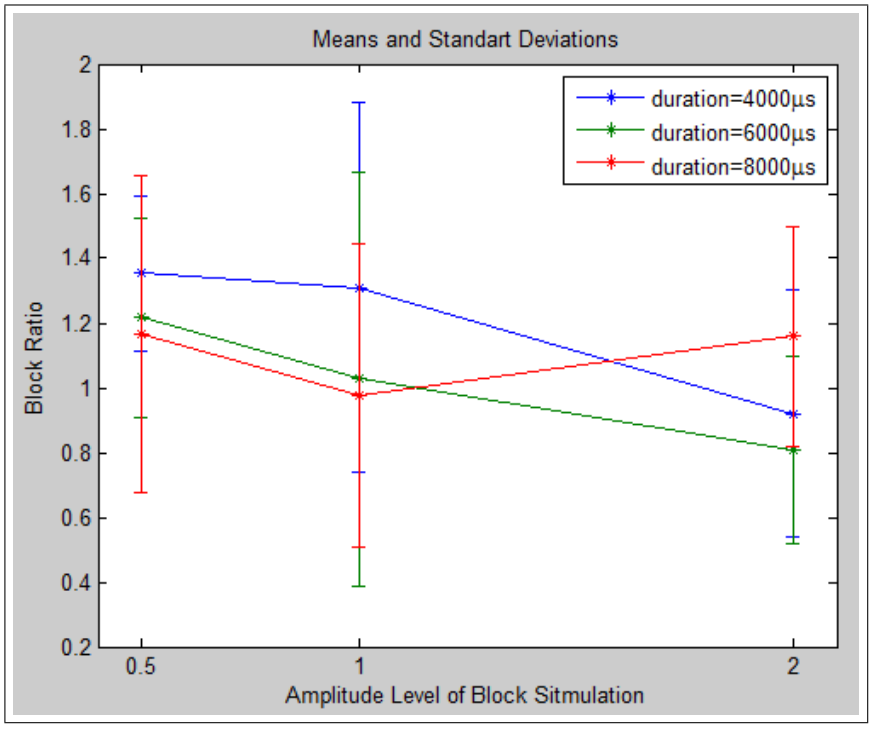

Figure 4.12 Means and standard deviations of block ratios at given block stimulation duration and amplitude level of block stimulation. Block ratios are the ratio of RMS of C component with the blocking stimulation to the RMS of C component evoked by pulse stimulation without block stimulation.

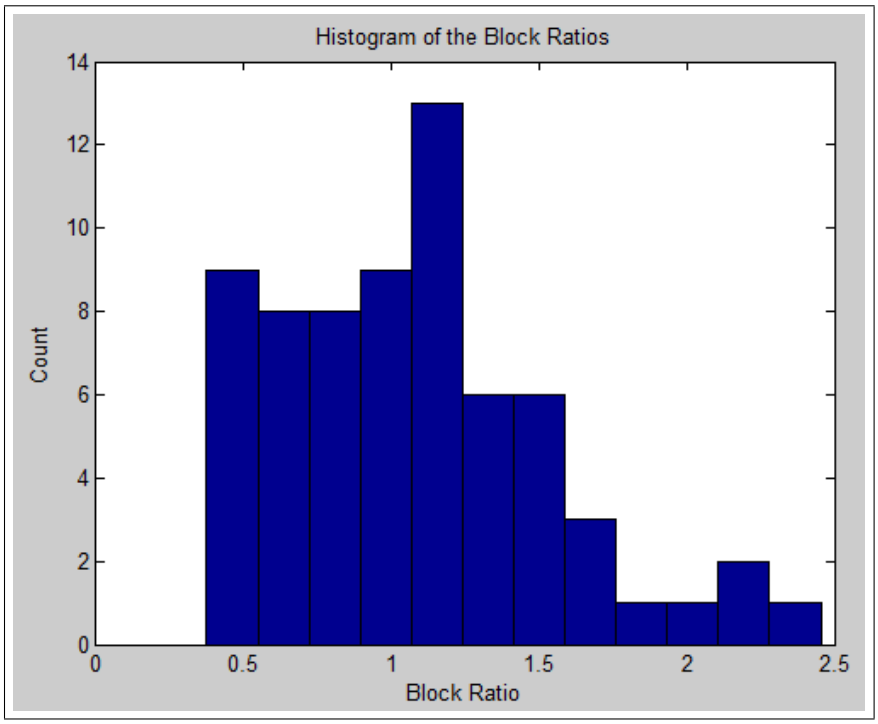

Figure 4.13 Histogram of the block ratios. A ratio smaller than one shows a blocking effect, that is to say, reduction of the C component.

5. DISCUSSION

5.1 Overview

It was shown that in some nerves and in some trials hyperpolarizing DC stimulation can block conduction in C fibers. In 44% of valid trails, the evoked C component was reduced. The C component was reduced in 9 subjects out of 14 (Table 5.1). The blocking stimulations were applied at levels which were multiples of the exaction current for 1 ms duration. Three levels of block amplitude were tested but a correlation did not find between block ratios of the C component after block to before block.

Table 5.1
The subjects in which the C component is reduced without evoking an A component.

C Block	No C Block
F141209L	F141202R
F141209R	F141218L
F141216L	F150306L
F150313R	F150324R
F150316L	F150325R
F150316R	
F150318R	
F150326L	
F150326R	

In addition, when the trials which had A fibers activation with the block were ignored the C block was achieved in 117 trial out of 292 trials. In this conduction, all subjects except F150324R were blocked. However, a successful blocking stimulation should not elicit A response while blocking the C fibers. The reason for this situation might be an unequal current share between anode electrodes in the tripolar configu-

ration. If the impedance were not equal for both electrodes, the necessary amplitude might not be reached at one anode. This electrode may elicit an A response. I investigated the effect of the blocking stimulation amplitude on this secondary A response. There was no correlation, although the literature states that increasing the amplitude of the block typically reduces the A component [26, 28, 29, 30, 76]. The discrepancy may be because of the block amplitudes. In this study the amplitudes were selected relative to the excitation current in the strength duration curve. However, studies in the literature used a fixed set of amplitudes. Additionally, the problems with the electrode design were not predictable. In another words, the impedance mismatch could vary from session to session.

When the hyperpolarizing stimulation stopped suddenly, the fibers can be activated. This phenomenon is traditionally called anodal break excitation. In order to avoid this effect, the blocking stimulation was diminished exponentially. The decay duration was determined in preliminary experiments and fixed to 5 ms. Different decay waveforms were tested in the literature, such as 10 ms rampes [29], exponential decay of 10 ms [28], 3-4 ms [30]. It was observed that 5 ms decay was appropriate in trials for which the block stimulation did not evoke A component. However, when the block stimulation caused activation in A fibers, it was observed that the decay duration was not adequate and the anodal break excitation always observed. It is important to note that these trials were excluded from the analysis of the C block ratios.

The conduction velocities were M: 41.06 m/s, SD: 1.67 and M:1.67 m/s, SD: 0.26 for A component and C component, respectively. The results are consistent with the literature as given in the Figure 5.1. On the other hand, there are some variations in literature [51, 52, 53]. The main reason of it must be because of experimental conditions and methods used to measure. The temperature affects the conduction velocity. Increase in temperature speeds up the conduction. And in this study, the positive peak of CAP components are used instead of single fibers.

The strength-duration curves were found for A components and C components of all subjects. The rheobases and chronaxies were derived from Weiss and Lapicque equations. The Lapicque equation estimated the rheobases slightly higher than the Weiss equation while the situation was opposite for chronaxies. The rheobase of the C components was 14 times of the A components. However, the expected ratio is the 2-3

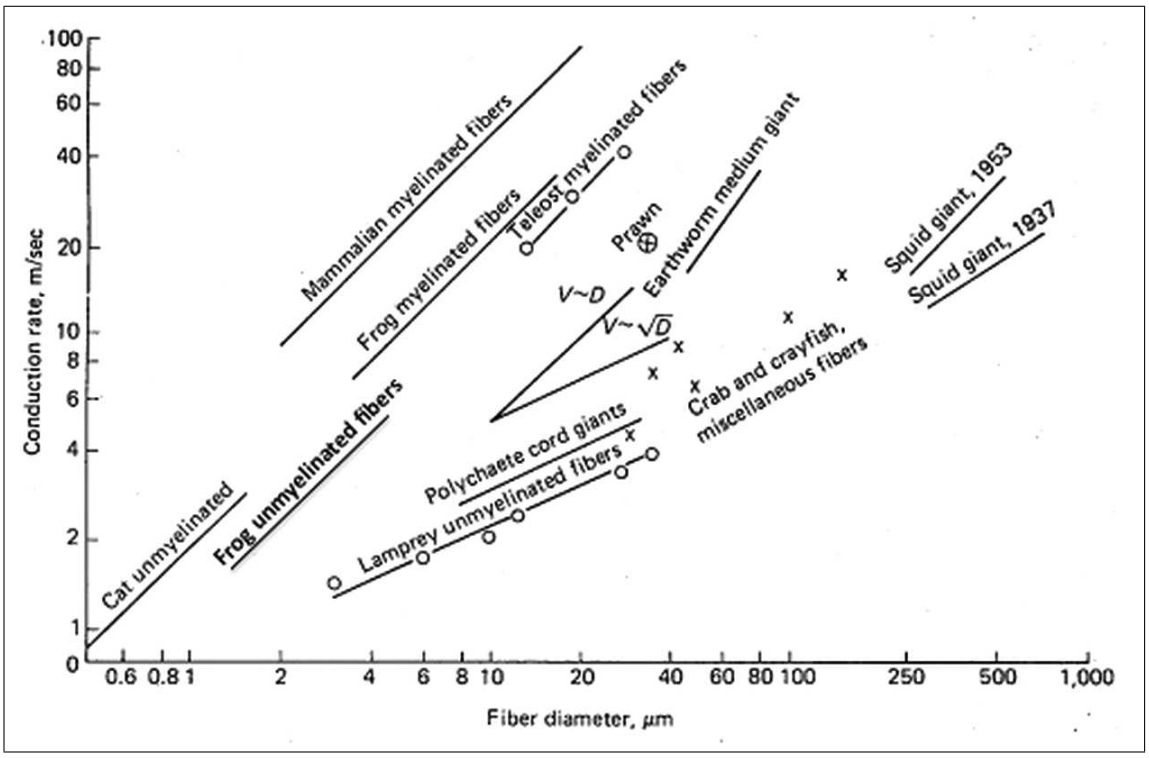

Figure 5.1 Conduction velocities of nerve fibers from different species [53].

folds [77] according to the literature. The rheobase is strictly depends on the contact between the electrodes and the nerve. If small contact area is established, the nerve will be stimulated with lower amplitudes because the current is focused. But such a difference reported here must result from the threshold criteria and the lack of very long stimulation durations. The longer stimulation durations would provide better estimation of rheobase. The chronaxies of the A components and C components were close each other. The chronaxie for A fibers of frog was reported as 50-300 μs and 3.5-5 ms for C fibers [53]. The chronaxies achieved in this study differ from the literature because of the threshold criteria and the electrode design.

5.2 Electrode Design and Technical Limitations

The electrode design, which was tested among other custom made alternatives, provided good surface contact with the nerve. The slight squeezing contact probably enabled the activation of deeper fibers in the nerve bundle. The diameter (25μm) of the

electrodes was selected to focus the current in a small area. The low rheobases for the C fibers may be considered to be evidence for a focused excitation. The tripolar design was used to reduce virtual cathode effect and prevented the propagation of action potential both directions. However, it did not work perfectly because it was handmade. A machine fabricated electrodes can provide better results. I was also observed that the squeezing design did not allow repositioning of the nerve because there was some crushing damage at that point. A design which controls the tightening force of the electrode may prevent this problem.

Two stimulators and an amplifier were used in this study and all were electrically isolated. The isolation assures the current flow between intended leads so the blocking stimulation current does not leak to the pulse stimulator. The pulse stimulator amplitude was set manually so it took a long time to derive the S-D curve. Software programmable stimulator would enable completely automatized test procedure so the experiment duration would be reduced. Additionally, to improve the performance of the tripolar configuration, a twin block stimulator may be used and the current through the anodes may be independently controlled.

5.3 Physiological Limitations

The locations of stimulation blocking and recording electrodes are important for optimizing the experiment protocol and achieving a high signal to noise ratio. As the distances increase between the stimulation and block, there is betters separation of A and C components. Therefore, the nerve was dissected as long as possible. However, for smaller frogs this design was not practical. In the future, an adjustable nerve chamber may be more useful.

The most important issue was the artifact caused by blocking stimulation. This changed some of our results by increasing RMS value in the blocked conditions. A better nerve chamber may also prevent this problem.

5.4 Practical Considerations and Future Work

The electrical blocking supposedly provides instantaneous effect and recovery without irreversible damage. The method described here can improve the use of prosthetics with sensory feedback. The distance between stimulating electrode and the blocking electrode plays critical role in order to better separation of slow and fast conductive fibers. The longer distance enables better separation. So the length of the stumps must be long enough. However, there is a trade-off. As the distance is increased, the delay and the duration of blocking stimulation must increase as well because the C component reaches the blocking site later so the period of the stimulation is limited. For example, when the block is positioned 40 mm away from the stimulation, the C component passes the blocking side in interval of 30-60 ms approximately. In this window, a stimulation which would activate A fibers is impossible in practice. As a result, the stimulation frequency is limited with 16 pulses per second. The repetition can be increased by shortening the distance. In order to avoid this trade-off, the blocking stimulation may be optional for the user and it is turned on when it is necessary. An improvement in the electrode design or by using spatially selective electrodes in the literature, the nonmyelinated fibers may be selected for the block only.

In future studies, the most crucial step is improvement of the blocking performance by the reducing artifact and preventing A fiber activation. As a preliminary test, this may be done by using commercial cuff electrode and a twin block stimulator. It may be also interesting to test the blocking effect in the other direction in the nerve. Due to branching, the morphology is not identical. However, the application was meant for the propagation toward the proximal direction. Lastly, a mammalian model may be used for future experiments. For example, the anatomy of rat nerves is similar to humans', who the real targets of neuroprosthesis.

REFERENCES

1. Ziegler-Graham, K., E. J. MacKenzie, P. L. Ephraim, T. G. Travison, and R. Brookmeyer, "Estimating the prevalence of limb loss in the united states: 2005 to 2050," *Archives of Physical Medicine and Rehabilitation*, Vol. 89, no. 3, pp. 422–429, 2008.

2. Tan, D. W., M. a. Schiefer, M. W. Keith, J. R. Anderson, J. Tyler, and D. J. Tyler, "A neural interface provides long-term stable natural touch perception," *Science Translational Medicine*, Vol. 138, no. 6, pp. 257ra138–257ra138, 2014.

3. Dhillon, G. S., and K. W. Horch, "Direct neural sensory feedback and control of a prothetic arm," *Neural Systems and Rehabilitation Engineering, IEEE Transactions*, Vol. 13, no. 4, pp. 468–472, 2005.

4. Raspopovic, S., M. Capogrosso, F. M. Petrini, M. Bonizzato, J. Rigosa, G. Di Pino, J. Carpaneto, M. Controzzi, T. Boretius, E. Fernandez, G. Granata, C. M. Oddo, L. Citi, a. L. Ciancio, C. Cipriani, M. C. Carrozza, W. Jensen, E. Guglielmelli, T. Stieglitz, P. M. Rossini, and S. Micera, "Restoring natural sensory feedback in real-time bidirectional hand prostheses," *Science Translational Medicine*, Vol. 6, no. 222, pp. 222ra19–222ra19, 2014.

5. Dhillon, G. S., T. B. Krüger, J. S. Sandhu, and K. W. Horch, "Effects of short-term training on sensory and motor function in severed nerves of long-term human amputees.," *Journal of neurophysiology*, Vol. 93, no. 5, pp. 2625–2633, 2005.

6. Miles, J., and S. Lipton, "Phantom limb pain treated by electrical stimulation," *Pain*, Vol. 5, no. 4, pp. 373–382, 1978.

7. Macefield, B. Y. G., S. C. Gandevia, and D. Burke, "Perceptual responses to microstimulation of single afferents innervating joints, muscles and skin of the human hand," *Physiology*, Vol. 429, no. 1990, pp. 113–129, 2009.

8. Kandel, E. C., J. H. Schwartz, T. M. Jessell, S. A. Siegelbaum, and A. J. Hudspeth, "The brain and behaviour," in *Principles of Neural Science*, ch. 1, pp. 5–19, New York: The McGraw-Hill Inc., 5th ed., 2013.

9. Vera-Portocarrero, L., "Brain development," in *Brain Facts* (Chudler, E. H., ed.), ch. 2, pp. 8–11, New York: Chelsea House, 2006.

10. Evans-Martin, F. F., and D. A. Cooley, "Organization of the nervous system," in *The Nervous System* (Mallon, T., ed.), ch. 3rd, pp. 31–51, New York: Chelsea House, 2004.

11. Silbernagl, S., and A. Despopoulos, "Nerve and muscle, physical work," in *Color Atlas of Physiology*, ch. 2, pp. 42–77, New York: Thieme, 6th ed., 2008.

12. Kandel, E. C., J. H. Schwartz, T. M. Jessell, S. A. Siegelbaum, and A. J. Hudspeth, "Nerve cells, neural circuitry, and behavior," in *Principles of Neural Science*, ch. 2, pp. 21–38, New York: The McGraw-Hill Inc., 5th ed., 2013.

13. Kandel, E. C., J. H. Schwartz, T. M. Jessell, S. A. Siegelbaum, and A. J. Hudspeth, "Membrane potential and the passive electrical properties of the neuron," in *Principles of Neural Science*, ch. 6, pp. 126–147, New York: The McGraw-Hill Inc., 5th ed., 2013.

14. Kandel, E. C., J. H. Schwartz, T. M. Jessell, S. A. Siegelbaum, and A. J. Hudspeth, "Sensory coding," in *Principles of Neural Science*, ch. 21, pp. 449–474, New York: The McGraw-Hill Inc., 5th ed., 2013.

15. Rattay, F., "The basic mechanism for the electrical stimulation of the nervous system," *Neuroscience*, Vol. 89, no. 2, pp. 335–346, 1999.

16. Durand, D. M., "Electrical stimulation of excitable tissue," in *The Biomedical Engineering Handbook* (Bronzino, J., ed.), ch. 17th, pp. 17.1–17.22, Boca Raton: CRC Press LLC, 2nd ed., 2000.

17. Geddes, L. a., and J. D. Bourland, "The strength-duration curve.," *IEEE transactions on bio-medical engineering*, Vol. 32, no. 6, pp. 458–459, 1985.

18. Shariat, A. N., P. M. Horan, C. McCally, and A. P. Frulla, "Electrical nerve stimulators and localization of peripheral nerves," *NYSORA*, Sept. 2013.

19. Kandel, E. C., J. H. Schwartz, T. M. Jessell, S. A. Siegelbaum, and A. J. Hudspeth, "The somatosensory system: receptors and central pathways," in *Principles of Neural Science*, ch. 22, pp. 473–497, New York: The McGraw-Hill Inc., 5th ed., 2013.

20. Perl, E. R., "Ideas about pain, a historical view.," *Nature reviews. Neuroscience*, Vol. 8, no. 1, pp. 71–80, 2007.

21. Mann, M. D., "Peripheral nerves," in *The Nervous System In Action*, pp. 12.1–12.8, 2011.

22. Kandel, E. C., J. H. Schwartz, T. M. Jessell, S. A. Siegelbaum, and A. J. Hudspeth, "Propagated signaling: the action potential," in *Principles of Neural Science*, ch. 7, pp. 148–171, New York: The McGraw-Hill Inc., 5th ed., 2013.

23. Petsche, U., E. Fleischer, F. Lembeck, and H. O. Handwerker, "The effect of capsaicin application to a peripheral nerve on impulse conduction in functionally identified afferent nerve fibres," *Brain Research*, Vol. 265, no. 2, pp. 233–240, 1983.

24. Tasaki, I., "Collision of two nerve impulses in the nerve fibre," *Biochimica et Biophysica Acta*, Vol. 3, pp. 494–497, 1949.

25. Mortimer, J. T., "A Technique for collision block of peripheral nerve : single stimulus analysis," *IEEE Transactions on Biomedical Engineering*, Vol. 5, no. 1, pp. 373–378, 1981.

26. Bhadra, N., and K. L. Kilgore, "Direct current electrical conduction block of peripheral nerve," *Rehabilitation*, Vol. 12, no. 3, pp. 313–324, 2004.

27. Tai, C., J. R. Roppolo, and W. C. De Groat, "Analysis of nerve conduction block induced by direct current.," *Journal of computational neuroscience*, Vol. 27, no. 2, pp. 201–210, 2009.

28. Accornero, B. Y. N., G. Bini, G. L. Lenzi, and M. Manfredi, "Selective activation of peripheral nerve fibre groups of different diameter by triangular shaped stimulus pulses.," *The Journal of physiology*, Vol. 273, no. 3, pp. 539–560, 1977.

29. Petruska, J. C., C. H. Hubscher, and R. D. Johnson, "Anodally focused polarization of peripheral nerve allows discrimination of myelinated and unmyelinated fiber input to brainstem nuclei," *Experimental Brain Research*, Vol. 121, no. 4, pp. 379–390, 1998.

30. Brindley, G. S., and M. D. Craggs, "A technique for anodally blocking large nerve fibres through chronically implanted electrodes.," *Journal of neurology, neurosurgery, and psychiatry*, Vol. 43, no. 12, pp. 1083–1090, 1980.

31. Fang, Z. P., and J. T. Mortimer, "Selective activation of small motor axous by quasitrapezoidal current pulses," *IEEE Trans Biomed Eng*, Vol. 38,No.2, no. 2, pp. 168–174, 1991.

32. Nikolski, V. P., A. T. Sambelashvili, and I. R. Efimov, "Mechanisms of make and break excitation revisited: paradoxical break excitation during diastolic stimulation.," *American journal of physiology. Heart and circulatory physiology*, Vol. 282, no. 2, pp. H565–H575, 2002.

33. Goodall, E. V., J. De Frits Breij, and J. Holsheimer, "Position-selective activation of peripheral nerve fibers with a cuff electrode," *IEEE Transactions on Biomedical Engineering*, Vol. 43, no. 8, pp. 851–856, 1996.

34. Kilgore, K. L., and N. Bhadra, "Reversible nerve conduction block using kilohertz frequency alternating current," *Neuromodulation*, Vol. 17, no. 3, pp. 242–254, 2014.

35. Tai, C., W. C. De Groat, and J. R. Roppolo, "Simulation analysis of conduction block in unmyelinated axons induced by high-frequency biphasic electrical currents," *IEEE Transactions on Biomedical Engineering*, Vol. 53, no. 7, pp. 1433–1436, 2006.

36. Joseph, L., and R. J. Butera, "High frequency stimulation selectively blocks different types of fibers in frog sciatic nerve," *Neural Systems and Rehabilitation Engineering, IEEE Transactions*, Vol. 19, no. 5, pp. 550–557, 2011.

37. Bowman, B. R., and D. R. McNeal, "Response of single alpha motoneurons to high-frequency pulse trains," *Stereotactic and Functional Neurosurgery*, Vol. 49, no. 3, pp. 121–138, 1986.

38. Tai, C., W. C. De Groat, and J. R. Roppolo, "Simulation of nerve block by high-frequency sinusoidal electrical current based on the Hodgkin-Huxley model," *IEEE Transactions on Neural Systems and Rehabilitation Engineering*, Vol. 13, no. 3, pp. 415–422, 2005.

39. Zhang, X., J. Roppolo, W. de Groat, and C. Tai, "Simulation analysis of nerve block by high frequency biphasic electrical current based on frankenhaeuser-huxley model.," in *Engineering in Medicine and Biology Society, 2005. IEEE-EMBS 2005. 27th Annual International Conference of the. IEEE*, Vol. 4, pp. 4247–4250, 2006.

40. Kilgore, K. L., and N. Bhadra, "Nerve conduction block utilising high-frequency alternating current," *Medical and Biological Engineering and Computing*, Vol. 42, no. 3, pp. 394–406, 2004.

41. Williamson, R. P., and B. J. Andrews, "Localized electrical nerve blocking," *IEEE Transactions on Biomedical Engineering*, Vol. 52, no. 3, pp. 362–370, 2005.

42. Ackermann, D. M., N. Bhadra, M. Gerges, and P. J. Thomas, "Dynamics and sensitivity analysis of high-frequency conduction block," *Journal of Neural Engineering*, Vol. 8, no. 6, p. 065007, 2011.

43. Agnew, W. F., D. B. McCreery, T. G. Yuen, and L. a. Bullara, "Histologic and physiologic evaluation of electrically stimulated peripheral nerve: considerations for the selection of parameters.," *Annals of biomedical engineering*, Vol. 17, no. 1, pp. 39–60, 1989.

44. Agnew, W. F., D. B. McCreery, T. G. H. Yuem, and L. A. Bullara, "Stimulation-induced axonal injury in peripheral nerve," *Muscle & Nerve*, Vol. 22, no. 10, pp. 1393–1402, 1999.

45. Miles, J. D., K. L. Kilgore, N. Bhadra, and E. a. Lahowetz, "Effects of ramped amplitude waveforms on the onset response of high-frequency mammalian nerve block.," *Journal of neural engineering*, Vol. 4, no. 4, pp. 390–398, 2007.

46. Ackermann, D. M., N. Bhadra, E. L. Foldes, and K. L. Kilgore, "Conduction block of whole nerve without onset firing using combined high frequency and direct current," *Medical and Biological Engineering and Computing*, Vol. 49, no. 2, pp. 241–251, 2011.

47. Gerges, M., E. L. Foldes, D. M. Ackermann, N. Bhadra, N. Bhadra, and K. L. Kilgore, "Frequency- and amplitude-transitioned waveforms mitigate the onset response in high-frequency nerve block.," *Journal of neural engineering*, Vol. 7, no. 6, pp. 066003–066012, 2010.

48. Frankenhaeuser, B., and a. F. Huxley, "The action potential in the myelinated nerve fibre of Xenopus laevis as computed on the basis of voltage clamp data," *The Journal of physiology*, Vol. 171, no. 2, pp. 302–315, 1964.

49. Egar, M., and M. Singer, "A quantitative electron microscope analysis of peripheral nerve in the urodele amphibian in relation to limb regenerative capacity.," *Journal of morphology*, Vol. 133, no. 4, pp. 387–397, 1971.

50. Linas, R., and W. Precht, "Electrophysiology of the peripheral myelinated nerve," in *Frog Neurobiology A Handbook*, ch. 1, pp. 3–32, New York: Springer, 1st ed., 1979.

51. Hutchinson, N. a., Z. J. Koles, and R. S. Smith, "Conduction velocity in myelinated nerve fibres of Xenopus laevis.," *The Journal of physiology*, Vol. 208, no. 2, pp. 279–289, 1970.

52. Buchanan, S., a. a. Harper, and J. R. Elliott, "Differential effects of tetrodotoxin (TTX) and high external K+ on A and C fibre compound action potential peaks in frog sciatic nerve.," *Neuroscience Letters*, Vol. 219, no. 2, pp. 131–134, 1996.

53. Bullock, T. H., and G. A. Horridge, "Comparative neurology of excitability and conduction," in *Structure and Function in the Nervous Systems of Invertebrates Vol.1*, ch. 3, pp. 124–166, London: W. H. Freeman and Company, 1st ed., 1965.

54. Leem, J. W., W. D. Willis, and J. M. Chung, "Cutaneous sensory receptors in the rat foot.," *Journal of neurophysiology*, Vol. 69, no. 5, pp. 1684–1699, 1993.

55. Navarro, X., T. B. Krueger, N. Lago, S. Micera, T. Stieglitz, and P. Dario, "A Critical review of interfaces with the peripheral nervous system for the control of neuroprotheses and hybrid bionic systems," *J Peripher Nerv Syst*, Vol. 10, pp. 229–258, 2005.

56. Krnjević, K., "The connective tissue of the frog sciatic nerve," *Quarterly journal of experimental physiology and cognate medical sciences*, Vol. 39, no. 1, pp. 55–72, 1954.

57. McGill University, "Compound action potential," in *The McGill Physiology Virtual Laboratory PHGY212 notes*, McGill University, 2005.

58. "Phrenic nerve stimulation for diaphragm pacing in a quadriplegic patient," *Journal of Korean Neurosurgical Society*, Vol. 54, no. 4, pp. 359–362, 2013.

59. Glenn, W. W., and M. L. Phelps, "Diaphragm pacing by electrical stimulation of the phrenic nerve," *Neurosurgery*, Vol. 17, no. 6, pp. 974–984, 1985.

60. Nashold, B. S., J. L. Goldner, J. B. Mullen, and D. S. Bright, "Long-term pain control by direct peripheral nerve stimulation," *The Journal of Bone & Joint Surgery*, Vol. 64, no. 1, pp. 1–10, 1982.

61. Strege, D. W., W. P. Cooney, M. B. Wood, S. J. Johnson, and B. J. Metcalf, "Chronic peripheral nerve pain treated with direct electrical nerve stimulation.," *The Journal of hand surgery*, Vol. 19, no. 6, pp. 931–939, 1994.

62. "Peripheral nerve stimulation for the treatment of chronic pain," *Journal of Clinical Neuroscience*, Vol. 14, no. 3, pp. 216–221, 2007.

63. Brindley, G. S., "The first 500 patients with sacral anterior root stimulator implants: general description.," *Paraplegia*, Vol. 32, no. 12, pp. 795–805, 1994.

64. Rijkhoff, N. J. M., "Neuroprostheses to treat neurogenic bladder dysfunction: Current status and future perspectives," *Child's Nervous System*, Vol. 20, no. 2, pp. 75–86, 2004.

65. Waters, R. L., D. R. McNeal, W. Faloon, and B. Clifford, "Functional electrical stimulation of the peroneal nerve for hemiplegia. Long-term clinical follow-up," *The Journal of Bone & Joint Surgery*, Vol. 67, no. 5, pp. 792–793, 1985.

66. Haugland, M. K., and T. Sinkjaer, "Cutaneous whole nerve recordings used for correction of footdrop in hemiplegic man," *IEEE Transactions on Rehabilitation Engineering*, Vol. 3, no. 4, pp. 307–317, 1995.

67. Triolo, R., C. Bieri, J. Uhlir, and R. Kobetic, "Implanted FNS systems for assisted standing and transfers for individuals with cervical spinal cord injuries," *Arch Phys Med Rehabil*, Vol. 77, no. 11, pp. 1119–1128, 1996.

68. Taylor, P. N., J. H. Burridge, A. L. Dunkerley, D. E. Wood, J. a. Norton, C. Singleton, and I. D. Swain, "Clinical use of the odstock dropped foot stimulator: Its effect on the speed and effort of walking," *Archives of Physical Medicine and Rehabilitation*, Vol. 80, no. 12, pp. 1577–1583, 1999.

69. Bajd, T., a. Kralj, M. Stefancic, and N. Lavrac, "Use of functional electrical stimulation in the lower extremities of incomplete spinal cord injured patients," *Artificial Organs*, Vol. 23, no. 5, pp. 403–409, 1999.

70. Nag, S., K. A. Ng, R. Jagadeesan, S. Sheshadri, I. Delgado-mart, S. Bossi, S.-c. Yen, and N. V. Thakor, "Neural prosthesis for motor function restoration in upper limb extremity," *In Biomedical Circuits and Systems Conference (BioCAS)*, Vol. IEEE, pp. 388–391, 2014.

71. Kilgore, K. L., H. a. Hoyen, A. M. Bryden, R. L. Hart, M. W. Keith, and P. H. Peckham, "An implanted upper-extremity neuroprosthesis using myoelectric control," *Hand, The*, Vol. 33, no. 4, pp. 539–550, 2009.

72. Bhadra, N., K. L. Kilgore, and P. H. Peckham, "Implanted stimulators for restoration of function in spinal cord injury," *Medical Engineering and Physics*, Vol. 23, no. 1, pp. 19–28, 2001.

73. Güçlü, B., "Low-cost computer-controlled current stimulator for the student laboratory.," *Advances in physiology education*, Vol. 31, no. 2, pp. 223–231, 2007.

74. Wobbrock, J. O., L. Findlater, D. Gergle, and J. J. Higgins, "The aligned rank transform for nonparametric factorial analyses using only ANOVA procedures," in *SIGCHI Conference on Human Factors in Computing Systems*, pp. 143–146, 2011.

75. Brunel, N., and M. C. W. Van Rossum, "Quantitative investigations of electrical nerve excitation treated as polarization," *Biological Cybernetics*, Vol. 97, no. 5-6, pp. 341–349, 2007.

76. Vučković, A., N. J. M. Rijkhoff, and J. J. Struijk, "Different pulse shapes to obtain small fiber selective activation by anodal blocking - A simulation study," *IEEE Transactions on Biomedical Engineering*, Vol. 51, no. 5, pp. 698–706, 2004.

77. Li, C. L., and A. Bak, "Excitability characteristics of the A- and C-fibers in a peripheral nerve.," *Experimental neurology*, Vol. 50, no. 1, pp. 67–79, 1976.